UNIVERSITAT POLITÈCNICA DE CATALUNYA
BARCELONATECH
Departament de Teoria del Senyal
i Comunicacions

IMPLEMENTING IMPROVEMENTS IN OBTAINING HIGH RESOLUTION SOIL MOISTURE MAPS USING SMOS

A Thesis submitted to the

Faculty of the Escola Tècnica Superior

d'Enginyeria de Telecomunicacions de Barcelona

Universitat Politècnica de Catalunya

by

Francesc Xavier Pou Ibar

Advisors: Mercedes Vall-llossera Ferrán

María Piles Guillem

Adriano Camps Carmona

Barcelona, July 2015

INDEX

FIGURE INDEX

TABLE INDEX

1. INTRODUCTION

Weather is a complex combination of different processes like wind, snow, rain and temperature that are crucial in order to understand its main changes. Soil moisture is a variable linking the Earth's water, energy and carbon cycles. Soil moisture measurements control the evaporation of water and it can help to detect specific areas with high risk of floods, droughts or forest fires among others. Soil moisture maps can help in preventing these natural disasters. It is already known that soil moisture and ocean salinity are crucial parameters for controlling hydrological cycles. Until very recently there were no global scale measurements of these two parameters because the technology was not prepared for sending a mission which could obtain maps with enough resolution. In November 2009, SMOS (Soil Moisture and Ocean salinity) mission was launched for measuring these two crucial parameters. SMOS is one of the ESA (European Space Agency) Earth Explorer mission included in the Living Planet Program (http://www.esa.int/Our_Activities/Observing_the_Earth/SMOS/).

AQUARIUS (launched in 2011) and SMAP (launched in January 2015) are the two USA missions devoted to salinity and soil moisture respectively. This means a significant improvement in climate predictions and also carries out innovations in remote sensing. Only by using Remote Sensing satellite missions it is possible to obtain maps at global scale regularly in small periods of time (for example, every 3 days).

This document has been divided in six chapters. In this chapter the objectives of the project are presented. In chapter two the bases of the radiometry are described. Chapter three is devoted to explain some actual Earth observation satellite missions and which products have been used or combined for obtaining geophysical parameters. In this project, 50km and 1km resolution Soil Moisture (soil moisture) maps have been used. In addition, chapter three presents the datasets provided by the different missions and the linking model and disaggregation method for soil moisture retrievals. Chapter four describes the interpolation techniques applied and analysed for increasing the spatial resolution of SMOS maps in all weather conditions. Chapter five presents an exhaustive analysis of the selected solution which combines the ERA-Interim data with the SMOS data. Finally, chapter six presents conclusions and future research lines.

1.1 OBJECTIVES OF THE PROJECT

The aim of this project is to improve the high resolution (1 km) soil moisture maps obtained from SMOS data and the application of a downscaling algorithm. In fact, until now, the methodology developed in UPC by Maria Piles in her thesis [1] for obtaining high resolution Soil Moisture combined the SMOS data at ~50km, Land Surface Temperature (LST) and Normalized Difference Vegetation Index (NDVI) from MODIS at high resolution (1km). Nevertheless, MODIS works at infrared frequencies, which are very affected by clouds and consequently no data is achieved on cloudy areas.

Consequently, the objective of this project is to obtain high resolution soil moisture maps with no holes on the cloudy areas. In addition, a validation work of these new maps has been required. 50Km resolution maps are very useful at global scale, but agricultural applications at regional scale needs higher resolution, such as 1km or less.

In order to achieve these objectives, different methods have been proven and their behaviour tested. Once the best methodology has been selected, the validation has been done using the in situ measurements on REMEDHUS site provided by University of Salamanca [2]. Also an inter-comparison between the new maps and the old SMOS L4 maps (1km resolution) was done on the areas where both had.

Finally, once validation results have been satisfactory, they have been uploaded on the geoportal of the SMOS-BEC (http://www.smos-bec.icm.csic.es/).

2. RADIOMETRY BASES

Most of the energy received in Earth belongs to solar electromagnetic radiation. Part of this energy is absorbed in the atmosphere and the remnant arrives to Earth surface, where part of it is absorbed and the other is reflexed. Energy absorption by substances also carries thermal energy changes which produce an increment in their temperatures. When equilibrium is reached, absorbed energy is then reemitted. All material media (gas, liquid or solid) radiate or emit electromagnetic energy, and Radiometry is the science that studies these phenomena.

In Radiometry, sensors working at different bands have been designed for different purposes. The parameter that characterizes the emission of the observed zone is called brightness temperature (T_B), which can vary from 0 K for a perfect reflector to T_{ph} for a perfect emitter. As the emissivity is defined as $e=T_B/ T_{ph}$, a perfect reflector such as a metallic object without loses has emissivity 0.

Radiometry is also known as passive remote sensing, because no power is emitted by the antenna, and only the spontaneous power emitted by the bodies is measured. It can be applied in radioastronomy, in monitoring the environment, but also for Earth observation from an airplane, fixed antennas or a satellite. Radiometric measurements can be obtained from different sensors at different frequencies. Increasing or decreasing the frequency of the antenna or the distance between its location and the measured point affects its size. Obtaining high resolution measurements from a satellite require much bigger antennas than measuring from an airplane for obtaining similar resolution for example. The only payload of SMOS is the MIRAS (Microwave Imaging Radiometer Aperture Synthesis) the first interferometric radiometer for earth observation. By the correlations between pairs of the small antennas distributed on three arms it simulates a bigger antenna and obtains maps at ~50km resolution.

2.1 BRIGHTNESS AND THERMAL RADIATION

Brightness [3] [4] is defined as the emitted power for unit solid angle and unit area and its units are W sr^{-1} m^{-2}. Considering that a surface radiates a power within the radiation diagram F_t (θ,ϕ), brightness will be defined as the expression (2.1), where A is the emitting surface and B (θ,ϕ) is the brightness at (θ, ϕ):

$$B(\theta,\phi) = \frac{F_t(\theta,\phi)}{A} \quad (2.1)$$

The received power for an antenna with a finite aperture (A_f):

$$P = F_t \frac{A_f}{R^2} = BA \frac{A_f}{R^2} = BA_r\Omega \qquad (2.2)$$

where Ω is the solid radiant surface angle detected by the receiving antenna, whose effective area is A_r.

The last expression assumes that the observation is taken from the maximum of the antenna's radiation diagram and that brightness is independent of frequency. When frequency dependence is considered, the total power received by an antenna over a bandwidth ∆f, extending from frequency f to a frequency f+ ∆f is given by

$$P = \frac{1}{2} A_r \int_f^{f+\Delta f} \iint_{4\pi} B_f\,(\theta, \phi) t(\boldsymbol{\theta}, \phi) d\Omega df \qquad (2.3)$$

where the solid-angle integration is carried out over all 4π steradiants, $t(\boldsymbol{\theta}, \phi)$ is the radiation diagram function, $B_f(\theta, \phi)$ is frequency dependant, $B_r(\theta, \phi)$ is defined as the bandwidth brightness and A_r is the receiving antenna area. If Bf is unpolarised (which is the case of atmospheric emission and many other surfaces), then, due to the fact that the antenna is polarized, the antenna will detect only half of the total power incident upon its surface, hence the factor ½ is introduced in equation (2.3). An example of radiation pattern for an antenna is shown in figure 2.1:

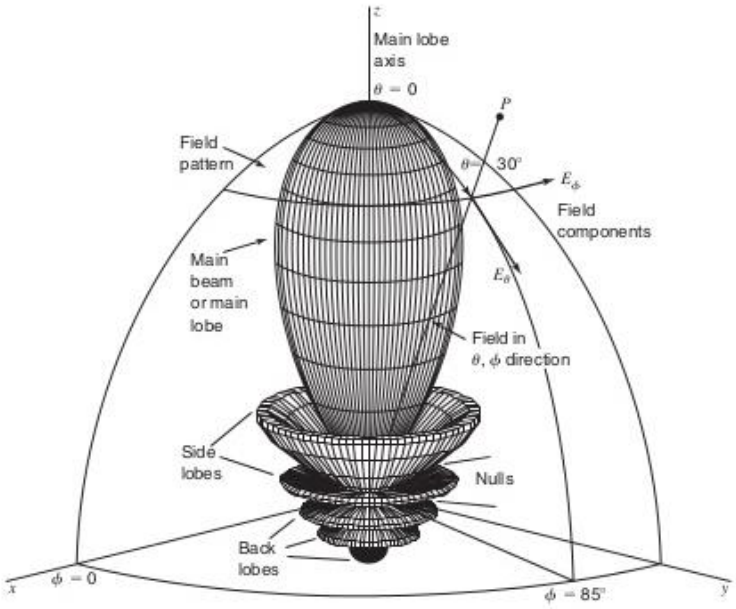

Fig. 2.1: Example of radiation pattern of an antenna [5]

2.2 BLACK BODY AND PLANCK'S LAW

A black body is defined as a body which absorbs and reemits all the power that reaches it and follows the Plank's Law. This body radiates uniformly in all directions with spectral brightness given by:

$$B_f = \frac{2hf^3}{c^2} \cdot \frac{1}{e^{\frac{hf}{k_B T_{ph}}} - 1} \quad (2.4)$$

where B_f is the blackbody spectral brightness in [W m^{-2} $sr^{-1}Hz^{-1}$], c=3x10^8 m/s is light velocity, h=6.63x10^{-34} joules is Planck's constant, k_B=1.38x10^{-23} joule K^{-1} is Boltzmann's constant, T_{ph} is the absolute temperature in Kelvin and f is frequency in Hz. Figure 2.2 shows the Planck's law radiation curves. It can be seen that brightness has dependence to frequency and temperature because it shows different behaviours for low and high frequencies. Figure 2.2 demonstrates that as temperature T increases the overall level of the spectral brightness curve increases and the frequency at which B_f is maximum also increases with T. On the other hand two very different behaviours can be observed for low and high frequencies. A comparison of Planck's law with its high-frequency and low-frequency approximations, known as Wien and Rayleigh-Jeans, respectively is provided by figure 2.3. Then, the spectral brightness for low frequencies (microwave region) can be approximated by Rayleigh-Jeans equation:

$$B_f = \frac{2K_B T}{\lambda^2} \quad (2.5)$$

For a blackbody at a room temperature of 300 K at frequencies lower than 117 GHz, the error for this approximation is lower than 1%.

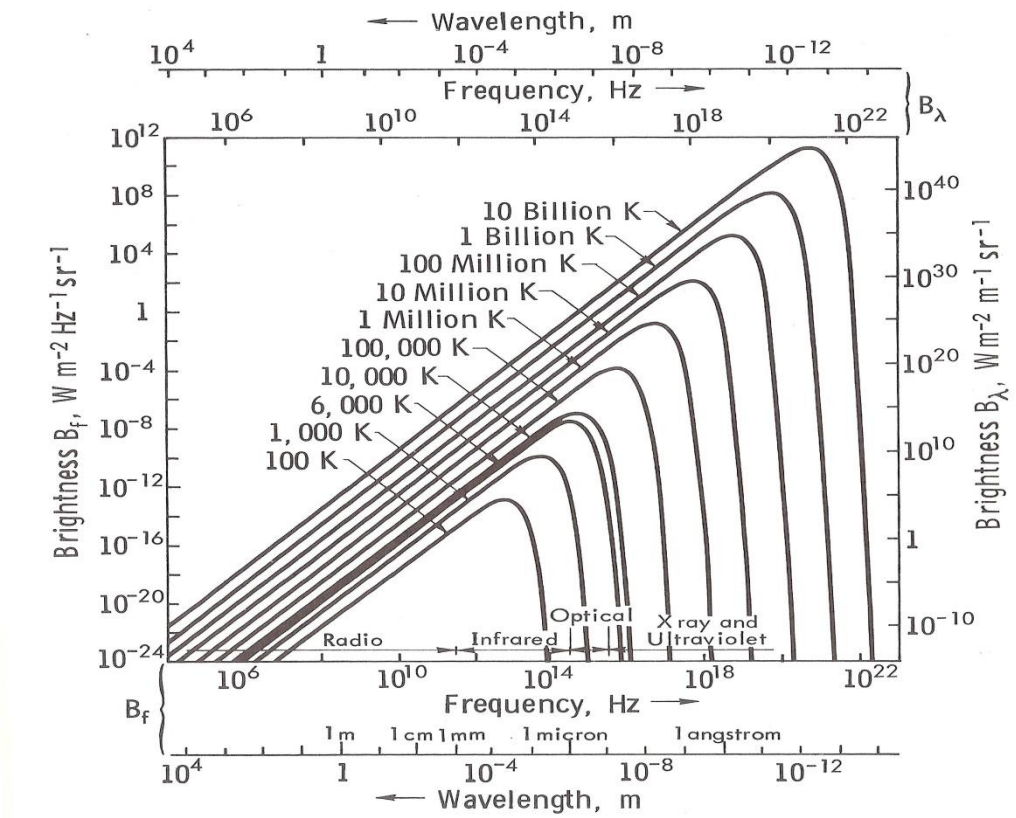

Fig. 2.2: Planck's Law radiation curves [4]

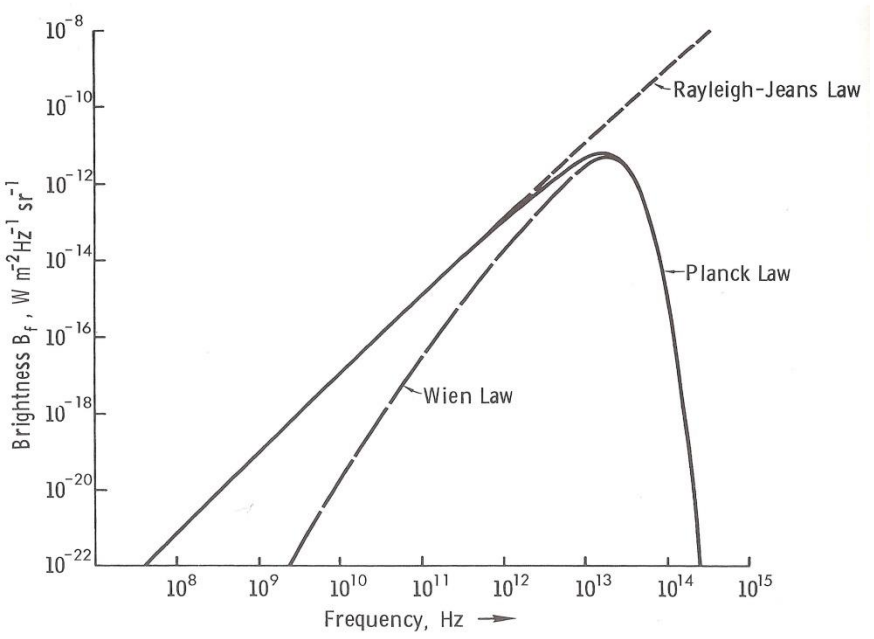

Fig. 2.3: Rayleigh-Jeans approximation (low frequencies) and Wien's Law (high frequencies). T=300K [4]

Finally, the expression (2.2) can be rewritten as follows:

$$P = K_B T \Delta f \quad (2.6)$$

This expression is used in remote sensing applications because it permits to consider a linear dependence between received power and temperature.

2.3 GRAY BODY

Black bodies are ideal bodies. In fact, real bodies absorb a part of the received energy and reflect the other amount. The absorbed power is reemitted and present directional properties. These materials are called gray bodies.

It can be observed that real materials radiate energy with directional dependence at each frequency. For this reason, measuring the emitted power at different frequencies and angles can help in determining geophysical properties of the measured area.

Brightness temperature can be defined as the physic temperature of an ideal black body that emits the same radiation diagram and spectrum as the gray body that is being measured. For this reason, brightness temperature associated to brightness is defined as:

$$T_B(\theta,\phi) = e(\theta,\phi)T \quad (2.7)$$

where $e(\theta,\phi)$ is defined as the emissivity and it has its lower value on 0 for a perfect reflectance and its higher value on 1 for a perfect emissivity. Then the spectral brightness for a gray body can be related to its brightness temperature as:

$$B = \frac{2K_B}{\lambda^2} T_B(\theta,\phi)\Delta f \quad (2.8)$$

T_B is the temperature a blackbody would have to produce the observed brightness $B(\theta,\phi)$, it is not the real temperature of the object, it is an effective temperature.

2.4 BRIGHTNESS APPARENT TEMPERATURE

The Brightness temperature is used for characterize the radiance for a real object (gray body). Similarly an apparent temperature is defined for characterizing the total brightness incident to a radiometer antenna $B_i(\theta,\phi)$ as:

$$B_i = \frac{2K_B}{\lambda^2} T_{AP}(\theta,\phi)\Delta f \quad (2.9)$$

Therefore the power collected by a radiometer antenna with a radiation pattern $F_n(\theta,\phi)$, which receive a gray body incidence brightness is given by:

$$P = \frac{1}{2} A_r \int_f^{f+\Delta f} \iint_{4\pi} \frac{2K_B}{\lambda^2} T_{AP}(\theta,\phi) F_n(\theta,\phi) d\Omega df \qquad (2.10)$$

It is useful to define an antenna temperature (T_A) as the equivalent temperature to the power received by the antenna, so that, it can be used the expression $P = K_B T_A \Delta f$. This antenna temperature is obtained as:

$$T_A = \frac{A_r}{\lambda^2} \iint_{4\pi} T_{AP}(\theta,\phi) F_n(\theta,\phi) d\Omega \qquad (2.11)$$

Hence, T_A includes contributions from the target observed as well as from radiation emitted and scattered from other sources, but not from internal elements.

Nowadays, one important application of passive remote sensing is Earth-looking from satellite. The antenna radiometer in this case is collecting radiation from both land surface and the atmosphere and may be expressed as:

$$T_{AP}(\theta,\phi) = T_{up} + (T_B + T_{sc}) \frac{1}{L_a} \qquad (2.12)$$

where T_B is the brightness temperature of the observed scene, T_{up} is the atmospheric upward radiation, T_{sc} is the downward atmospheric radiation scattered by the Earth in the direction of the antenna, and L_a represents the atmosphere attenuation.

2.5 LAND COVERS EMISSIVITY

The emissivity of the surface [6] [7] depends on its dielectric constant, which in turns depends on moisture content soil type, soil temperature, roughness and vegetation canopy among other factors. In order to obtain soil moisture from radiometric measurements all these effects must be taken into account. In fact, different approximations are used depending on the characteristics of the studied area.

2.5.1 Thermal radiation

In section 2.3 thermal radiation has been defined by physical temperature (T) and emissivity (e), which is related by the reflectivity (Γ_s) as:

$$T_B = e \cdot T \quad (2.13)$$

$$e = 1 - \Gamma_s \quad (2.14)$$

The reflectivity of a flat surface and a medium with uniform dielectric constant depends on the polarization (h,v) and the incidence angle as the Fresnel reflection coefficients:

$$\Gamma_v = \left| \frac{\varepsilon \cos\theta - \sqrt{\varepsilon - \sin^2\theta}}{\varepsilon \cos\theta + \sqrt{\varepsilon - \sin^2\theta}} \right|^2 \quad (2.15)$$

$$\Gamma_h = \left| \frac{\cos\theta - \sqrt{\varepsilon - \sin^2\theta}}{\cos\theta + \sqrt{\varepsilon - \sin^2\theta}} \right|^2 \quad (2.16)$$

where θ is the incidence angle and ε is the dielectric complex constant of soils.

2.5.2 Surface roughness

The effect of surface roughness on the microwave emission from bare soils is illustrated in figure 2.4. Experimental data from measurements at 1.4 GHz for three fields with different surface roughness conditions are plotted. It shows that surface roughness increases the emissivity of natural surfaces and reduces the difference between the vertical and the horizontal polarizations.

The effect of soil surface roughness on the emissivity has been widely studied and different approaches have been proposed to modify the reflectivity in (2.15) and (2.16) for rough surfaces. A simple semi-empirical expression for rough surface reflectivity was defined in Choudhoury et al, 1979 [8]:

$$\Gamma_s = \Gamma_{v,h} \cdot e^{-h_s \cdot \cos^2\theta} \quad (2.17)$$

where $\Gamma_{v,h}$ is the reflectivity given by Fresnel coefficients for vertical (v) and horizontal (h) polarizations, h_s=4k$^2\sigma^2$ is the soil parameter related to electromagnetic wave number (k) and standard deviation of the surface height (σ).

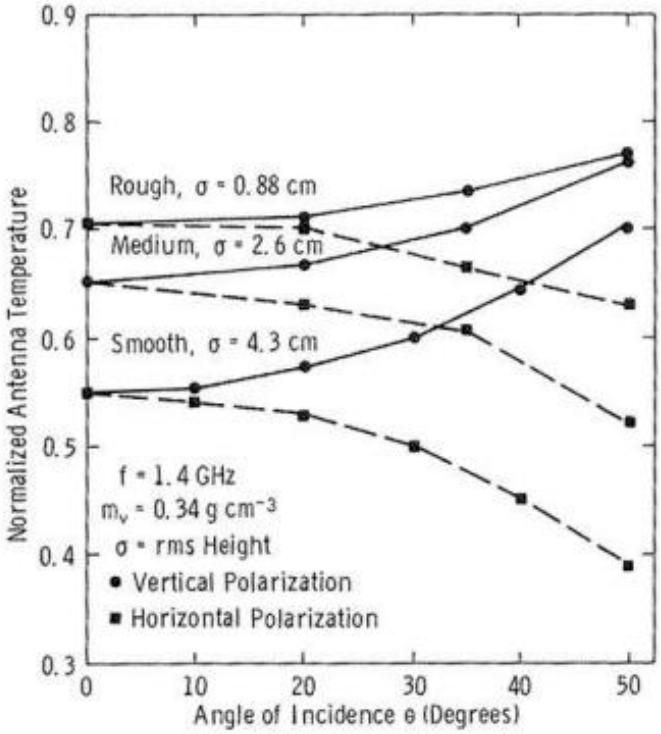

Fig. 2.4: Normalized antenna temperature at 1.4GHz respect to incidence angle for three types of terrain and different surface roughness conditions [9]

There is a more complex expression [10] where angular dependence of roughness and polarization mixing are taken into account:

$$\Gamma_s(\theta) = [(1-Q)\Gamma(\theta) + Q\Gamma(\theta)] \cdot e^{-h_s \cdot \cos^n \theta} \qquad (2.18)$$

Where Q models the effect of polarization mixing and n represents the angular dependence. A study made by Wigneron et al, 2001 [11] about soil roughness effects showed that Q and n could set equal 0 at L band and the h_s could be estimated semi-empirically, comprising most surface roughness conditions. Typical values for h_s range from 0.2 for smooth surfaces to 1 for a rough ploughed field.

2.5.3 Vegetation canopy

If the soil is covered by vegetation, the emission is affected by the canopy layer, which absorbs and scatters the radiation emanating from the soil and also adding its own contribution. Dense canopies can mask emitted soil radiation and the observed emissivity will be due to the vegetation. The absorption of the canopy layer depends on the frequency and the vegetation water content. Some models have been developed for accounting for the vegetation effect. The radiation from the land surface as observed from above the canopy is commonly expressed by a simple radiative transfer equations known as the τ-ω model by Mo et al., 1982 [12]:

$$T_B = e_p T_s \gamma + (1-\omega) T_v (1-\gamma) + \left(1-e_p\right)(1-\omega) T_v (1-\gamma)\gamma \qquad (2.19)$$

$$\gamma = e^{-\tau/\cos\theta} \qquad (2.20)$$

where T_s and T_v are the soil and vegetation effective temperatures, γ is the vegetation layer transmissivity and ω is the single scattering albedo. This equation combines the radiation from the soil attenuated by the vegetation (first term), the upward radiation directly from vegetation (second term) and downward radiation from the vegetation, reflected upward from the soil and attenuated by the canopy. γ depends on the vegetation optical depth τ and the incidence angle:

$$\gamma = \exp\left(-\frac{\tau}{cos\theta}\right) \qquad (2.21)$$

The optical depth is related to the vegetation density and frequency and can be linearly related to the vegetation water content VWC [kg/m^2] at L band with the empirical parameter b as demonstrated by Van de Griend and Wigneron, 2004 [13]:

$$\tau = b \cdot VWC \qquad (2.22)$$

In addition optical depth can be related [14] to the Normalized Difference Vegetation Index (NDVI):

$$\tau = \alpha + \beta \cdot (1 - \log NDVI) \qquad (2.23)$$

3. LINKING MODEL AND DISAGGREGATION METHOD

The SMOS mission objective was to provide the first ever global soil moisture measurements from L band observations, with an accuracy of 0.04 m^3/m^3 over 50 x 50 km^2 every 3 days. The spatial resolution of tens of kilometres is adequate for many global applications, but it is useless for other regional scale applications. Most hydrological processes occur at resolutions better than 1-10km.

Maria Piles in his thesis [1] proposed a downscaling approach to improve the spatial resolution of SMOS soil moisture estimates with the use of higher resolution visible/infrared satellite data. The algorithm is based on the so-called "universal triangle" that relates visible/infrared data, such as NDVI and Land Surface Temperature (LST) to the soil moisture status. It combines the high soil moisture accuracy of SMOS with the higher spatial resolution of the auxiliary data. Results showed good agreement with in-situ measurements at REMEDHUS site.

In this chapter soil moisture retrieval and disaggregation method are presented. First of all the data used are presented. After, the soil moisture retrieval algorithm and the disaggregation method applied for increasing spatial resolution are presented.

3.1 USED DATABASES

Satellite missions and REMEDHUS cal/val site are introduced in the following subsections.

3.1.1 SMOS mission

SMOS [15] is a Helio-synchronous polar orbit satellite located at an elevation of 758 km with a maximum revisit time of 3 days. The SMOS payload is the MIRAS (Microwave Imaging Radiometer Aperture Synthesis) instrument, which is the first interferometric radiometer [16] with a Y shape and 69 antennas distributed on the three arms and the central structure (see figure 1.1). MIRAS works at 1.4 GHz, in the protected L band. At L band, the atmosphere is almost transparent and signal emitted by earth is much less affected by vegetation than other bands such as infrared or optical. SMOS resolution (~50Km) is enough for global scale application such climatology; meanwhile for local or regional application much higher spatial resolutions are needed. In order to obtain higher resolutions, a combination between SMOS observations with data from other sensors at higher resolutions such as Land Surface Temperature and NDVI from MODIS (sensor aboard AQUA and TERRA satellites) have been developed.

SMOS mission products (available at http://cp34-bec.cmima.csic.es/data/) are divided in four different levels (Zundo et al, 2005)[17]:

- Level 0 products consist of raw data with added Earth Explorer headers. They include satellite data and calibration data from correlators.
- Level 1 products are divided into three categories:

- Level 1a products include calibrated visibilities (cross-correlations) for snapshot.
- Level 1b products radiometrically corrected and calibrated brightness temperatures maps for snapshot. These maps are referred to the antenna polarisation reference frame (T_{xx}, T_{yy} and T_{xy} for both dual-polarimetric and ful-polarimetric modes).
- Level 1c products are maps of brightness temperatures based on the swath. They are generated on a fixed grid on an Earth ellipsoid (T_{hh}, $T_{vv,}$ and $T_I = T_{hh} + T_{vv} = T_{xx} + T_{yy.\ Land}$ and sea products are produced separately.

- Level 2 products swath based maps of soil moisture or ocean salinity, computed from Level 1c products. Algorithms for mitigation Faraday rotation, Sun/Moon/galactic glint, atmospheric attenuation, etc., are already applied separately for soil moisture and ocean salinity.
- Level 3 products are the result of spatial-temporal aggregation of Level 2 data.
- Level 4 products use auxiliary data from other sources to combine with Level 2 or 3 SMOS products for obtaining improved products, suxh as high resolution maps for soil moisture.

The identification of these products will be done hereafter as L0, L1a, L1b, L1c, L2, L3 and L4, Level 0, Level 1a, Level 1b, Level 1c, Level 2, Level 3 and Level 4, respectively.

Fig. 3.1: SMOS mission [SMOS BEC [18]].

3.1.2 AQUA mission

AQUA [19] [20] satellite is a Sun-synchronous orbit satellite located at an elevation of 705 km and a revisit time similar to SMOS. The AQUA payload are the infrared sensors

AIRS, AMSU, AMSR-E, HSB, CERES, MODIS for cloud formation, precipitation and radiative properties, air-sea fluxes of energy, carbon, and moisture respectively, and AMSR-E for sea ice concentrations and extents. MODIS (Moderate Resolution Imaging Spectroradiometer) [21], has provided LST and NDVI data for increasing the spatial resolution of the soil moisture maps from SMOS measurements. It has been selected among other alternatives for its temporal resolution (1-2 days), data availability (near real time) and spatial resolution (1km). MODIS works at frequencies located in infrared and near infrared bands, so it is not able to get data from spots covered by clouds because the atmosphere is not transparent at these frequencies.

Fig. 3.2: AQUA mission [NASA [22]]

3.1.3 ERA-Interim database

ERA-Interim [23] is a global atmospheric reanalysis that, using improved atmospheric models, provides a wide range of climate variables [24] four times a day, as ice coverage, wind speed, soil moisture and temperatures among others, from 1979 to 2014. The spatial resolution of the dataset is approximately 80 km on 60 vertical levels but, using interpolations, it can be downloaded from its webpage at a resolution of 12.5 km. The global coverage of the dataset can provide data in four different hours, which are 6h, 12h, 18h and 00h.

SKIN or L1 temperatures from ERA-Interim have been used as a substitute to LST MODIS in the downscaling algorithm to combine with SMOS L2 data in order to increase the spatial resolution. These products are not affected by clouds.

3.1.4 In situ measurements on REMEDHUS

REMEDHUS [25] (Red de Estaciones de Medición de la Humedad del Suelo) is a set of stations located in different parts of the provinces of Zamora, Valladolid and Salamanca where daily in situ soil moisture and temperature measurements are obtained. This validation/calibration area belongs to *Grupo de Investigación en Recursos Hídricos de la Universidad de Salamanca (HIDRUS)*. The stations are

strategically located for measuring areas with different characteristics at a height between 700 and 900 meters (see figure 3.3). Each of them consists of 4 TDR probes, which measure the moisture content, inserted horizontally at 5, 25, 50 and 100 cm respectively.

This site is used for calibration and validation for both SMOS and SMAP missions.

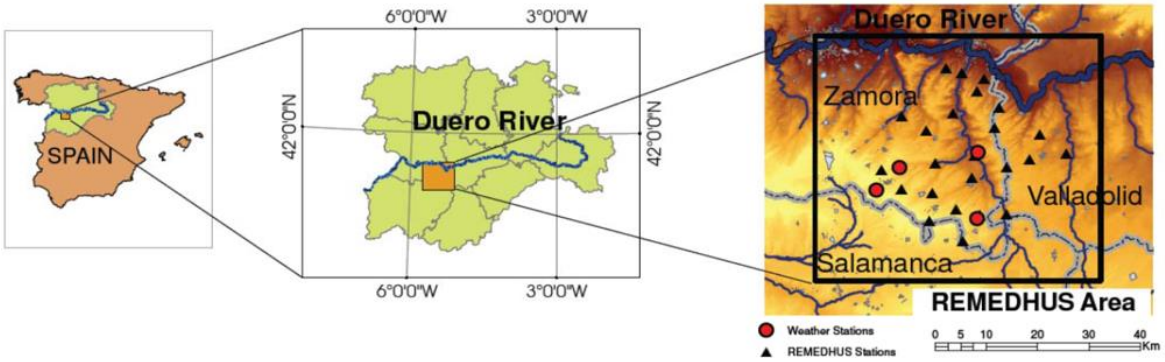

Fig. 3.3 Map of REMEDHUS area. Triangles refer to measure stations and circles to weather stations [MDPI [26]]

Figure 3.3 places this site on the Iberian Peninsula map and also the position of the 23 stations is settle on the area. In this project 19 of the 23 stations have been selected to characterize the whole area of REMEDHUS. They comprise the four types of terrain that have been studied, which are rainfed, fallow, vineyard and forest-pasture. Depending on the year, the terrain type can change, so the station located in that specific region can obtain measures of different types of terrain. In the Annex the usage of each station for every year can be found.

3.2 SOIL MOISTURE RETRIEVAL

The brightness temperature of soil depends on many variables, the most important are soil moisture, soil roughness (parameterized by h_s), soil temperature (LST) and vegetation characteristics such as albedo (ω) and opacity (τ). In order to retrieve soil moisture different techniques have been developed [27] [28]. Some of them work locally, other need a training phase or use of neural networks that will not be discussed here. The algorithms used by SMOS and SMAP only passive product are based on the inversion of geophysical model functions. The SMOS retrieval algorithm full uses the multi-angular observations for both dual-polarimetric and full-polarimetric modes. The retrieval algorithm of SMOS consists of inverting a geophysical model which finds a set of five input variables soil moisture, soil roughness, soil temperature, albedo and opacity which combination generates a brightness temperature that is the best match to the measured brightness temperature. Assuming that the errors are Gaussian, the inversion is performed by optimizing the cost function for weighted square differences between model and measured data:

$$Cost\ function = (F_{me} - F_{mo})^T C_F^{-1}(F_{me} - F_{mo}) + (p_i - p_{i0})^T C_p^{-1}(p_i - p_{i0}) \quad (3.1)$$

where F_{me} and F_{mo} are vectors containing microwave radiometer observations measured by MIRAS, C_F is the covariance matrix of the observations, p_i are the retrieval parameters that could influence the brightness temperature, p_{i0} are prior estimates of parameters p_i obtained from other sources and C_p is a diagonal matrix containing variances of the prior estimates.

This model has been demonstrated really robust by using field campaign and synthetic model-generated data. The main problem is that radiometer observations must be combined with auxiliary data in the inversion process to achieve accuracy and the retrieval setup needs to be optimized. Timely studies contributed to consolidate SMOS soil moisture retrieval algorithm.

3.3 DISAGGREGATION METHOD

In order to increase the spatial resolution of SMOS Soil Moisture maps a downscaling model which combine SMOS data with data at higher resolution from other sensors such as MODIS is necessary. Maria Piles, in her Ph. D Thesis [1], proposed the linking model based on SMOS data and higher spatial resolution of LST (Land Surface Temperature) and NDVI (Normalized Difference Vegetation Index) from MODIS. This algorithm is better described at chapter four. In SMOS BEC [29] (SMOS Barcelona Expert Center), these algorithms are computed and soil moisture maps at 1km resolution can be download from the geoportal http://cp34-bec.cmima.csic.es/. This high resolution Soil Moisture retrieval is a Level 4 product, because is obtained by the combination of measurements from two or more sensors or databases.

The only drawback of this technique is that spots covered by clouds cannot be retrieved at high resolution because MODIS data is affected by them. The main objective of this project was to obtain high resolution maps in all-weather conditions. In chapter five, it is demonstrated that the introduction of ERA-Interim dataset solves the problems related to atmosphere conditions dependence using the disaggregation method too.

The downscale methodology that has obtained the best results for SMOS is governed by the equation 3.2, presented in the article “A downscaling approach for SMOS land observations: evaluation of high resolution soil moisture maps over the Iberian Peninsula” [1]:

$$sm_{HR} = a_1 \cdot mask_{HR} + a_2 \cdot LST + a_3 \cdot NDVI + a_4 \cdot TBH + a_5 \cdot TBV \quad (3.2)$$

where the elements involved in the equation are:

- sm_{HR}: It corresponds to the value of soil moisture content at high resolution. Besides, as this equation is solved two times (one time at low resolution and one time at high resolution as it will be explained in 4.2), it also corresponds to the value of humidity at low resolution. For the soil moisture at low resolution it have been used first L2 SMOS files that are computed at the European Space Agency (ESA) and received at the SMOS-BEC in real time. These files have ~40 km resolution and are used to obtain the coefficients which then are applied to achieve high resolution maps from low resolution. By using SMOS L2 products, it has been proved that ERA-Interim files present better results than SMOS L4 and then, they have been replaced by SMOS L3 products [30], also of soil moisture at low resolution but in this case at the EASE-ML grid, which is 25 km. These products are worldwide and, when located inside the algorithm, are masked in order to use only the desired region. Figure 3.4 and 3.5 show the same region for SMOS L2 and L3 soil moisture products respectively. L3 products have less empty areas because its resolution is more accurate:

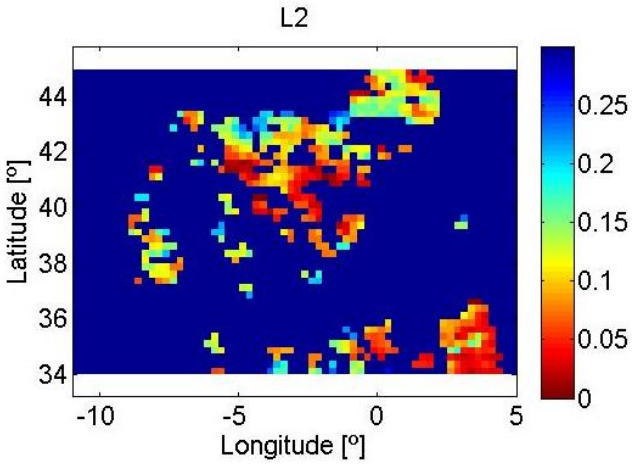

Fig. 3.4: April 2013 the 23th L2 soil moisture map provided by SMOS

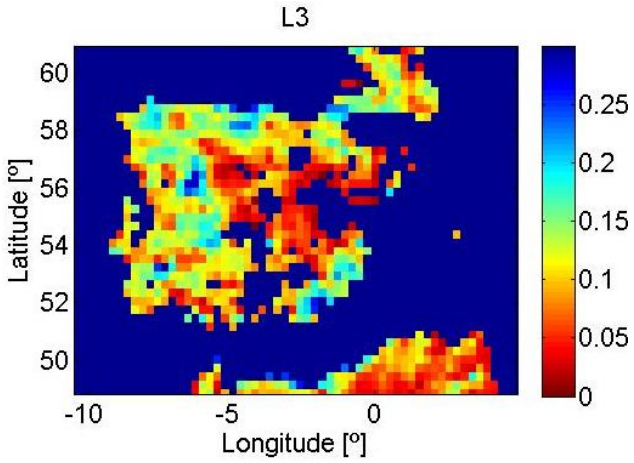

Fig. 3.5: April 2013 the 23th L3 soil moisture map provided by SMOS-BEC

- $mask_{HR}$: This element gives the number of equations to be solved in order to obtain high resolution soil moisture maps and also serves to mask earth-sea pixels.

- LST: Land Surface Temperature can be obtained from different resources. One source was the MYD11A1 [31] product provided by MODIS. But it has the

drawback it is affected by the clouds. Other sources, proposed in this project can be SKIN temperature and L1 temperature products provided by ERA-Interim. These are the products referring to the surface temperature of the Earth (SKIN) and the temperature at a depth from 0 to 7 cm (L1). Their original resolution is 80 km, but they can be downloaded at 12.5 km through interpolations from their own website [24]. The products are obtained every 6 hours and have the advantage of not being affected by the clouds. Figure 3.6 shows MODIS MYD11A1 product and its problem of being affected by clouds:

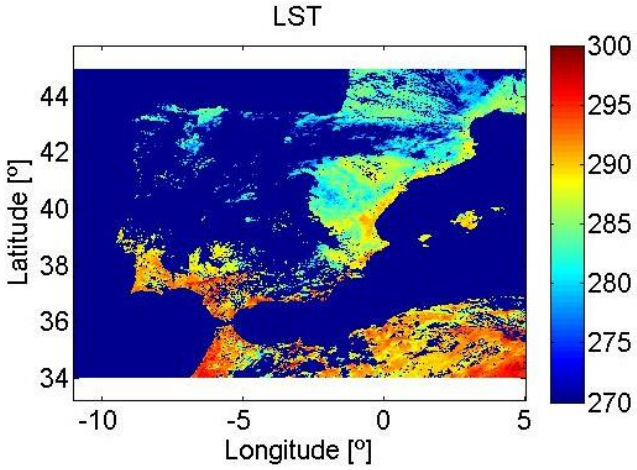

Fig. 3.6: January 2013 the 11th Land Surface Temperature map over the Iberian Peninsula provided by MODIS

- *NDVI*: The Normalized Difference Vegetation Index is the normalization of the relationship between the reflectance of the NIR band and the Red band. It is designed to have standard values between -1 and 1. The product used in this study is the MOD13A2 [32] [33], which has a resolution of 1 km and it is provided every 16 days. Being a relationship between the reflectance, the advantage provided is that it is not affected by the problem of clouds and therefore provides maps completely filled in the area covered by satellite passes. Due to its resolution (1 km), it is one of the elements that allow increasing the resolution of the computed soil moisture maps. This index can be provided by MODIS.

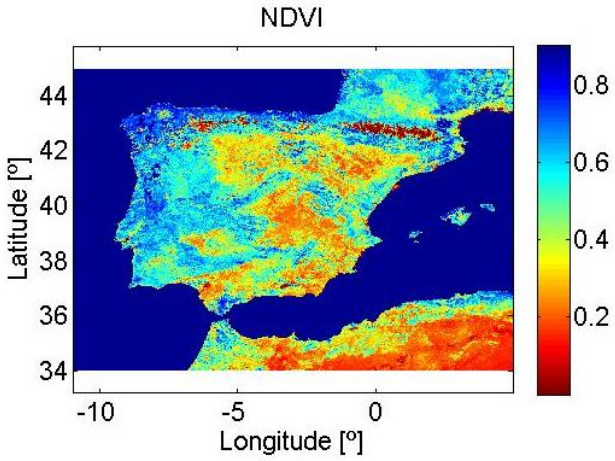

Fig. 3.7: Last 16 days of 2013 NDVI map over the Iberian Peninsula provided by MODIS

- $\boldsymbol{TBH\ and\ TBV}$: These elements correspond to brightness temperatures in both horizontal and vertical polarizations respectively. They are used to derive brightness temperature maps horizontally and vertically polarized for incidence angles of 32.5°, 42.5° and 52.5º and they bring the emission intensity of the studied area. Initially, the files that provide these values are not set in the resolution of 1 km. They are provided by SMOS.

- $\boldsymbol{a_n}$**:** They are the coefficients associated with each element of the equation. They arise from the matrix diagonalization solution. They are used as weighting factors for each variable contribution to the equation.

3.3.1 Algorithm description

Expression (3.2) is computed as follows:

First of all, data files corresponding to the day of interest are read and they provide the necessary variables, which are soil moisture L3, brightness temperatures, land surface temperatures and normalized difference vegetation indexes.

Some days have no soil moisture data maps at low resolution (level 2 products), consequently, no high resolution map can be computed. Table 5.7 identify those days on the Iberian Peninsula study, for SMOS lifetime from 2010 to 2014, both included.

Once the variables are collected, the algorithm calculates spatial resolution meshes and the distance to the coast in order to mask sea pixels. The algorithm applies EBI (equivalent background illumination), which in turn serves to improve RFI and the samples on the coastline. At this point, meshes at low and high resolution are created.

Finally, the algorithm based on least squares method is applied firstly in low resolution, using SMOS L2 or L3 products in order to obtain coefficients a_n. Once this model is built, these coefficients are applied to the equation (3.2) and the value of soil moisture at high resolution for each pixel is obtained.

4. INTERPOLATION APPROACH FOR IMPROVING HIGH RESOLUTION SOIL MOISTURE MAPS

The first high resolution soil moisture maps were obtained combining SMOS soil moisture L2 or L3 product (~ 50km resolution) with LST and NDVI (1km resolution) from MODIS sensor. Nevertheless, as it has been described in previous chapters, these maps could not be completed on areas covered by clouds. Infrared and near infrared bands, used by MODIS are very affected by atmospheric conditions such as clouds. The aim of this project was to fill these area without high resolution data. Different interpolation algorithms have been explored to solve this problem. They will be described in this chapter.

4.1 DATA USED

The only product used for this study is the SMOS L4 maps. The objective was to analyze if the spatial and/or interpolation techniques applied to L4 maps can obtain totally filled maps for all weather conditions.

The SMOS L4 product [29] is generated in the SMOS-BEC combining SMOS L2 maps with surface temperature of the Earth (LST) and NDVI provided by MODIS and applying algorithms to solve equation 3.2. The methodology is described in more detail in the previous chapter. SMOS L4 provides soil moisture daily data at the resolution of 1 km for both ascending and descending satellite passes with a maximum difference of 12 hours between them. The maps used in this study include the Iberian Peninsula and northern part of Africa; hence it covers inside longitudes from -5° to 11° and latitudes from 34º to 45º. Nevertheless, those high resolution maps can be obtained in any area of the world. September 2013 and February 2014 have been the two temporal windows used for this study.

4.2 METHODOLOGY AND RESULTS

For this particular study, only SMOS ascending passes for September 2013 and February 2014 have been used. Different interpolation techniques have been explored.

4.2.1 Monthly average maps

The first alternative analyzed was the interpolation based on a monthly averaged high resolution soil moisture map. The mean is computed from all the available values for each pixel on the map. As a first approximation the areas where no high resolution data is available are filled up with these mean values. Nevertheless, in many maps some artifacts appeared in the image because the great differences between real soil moisture values and monthly average values, in fact in general it is a very coarse approach.

4.3.1 Monthly average maps

When analyzing the evolution of the gaps on the high resolution maps along the year different behaviors have been observed. These behaviors are very dependent on the year's season. In particular, for February of 2014 there were soil moisture maps over the Iberian Peninsula for 22 days and for September of 2013 there were 26 days of data. But, in the first case, there were areas with no data in all the maps or only few days had data. The average value was only computed when data for 5 days or more was available. Figure 3.1 shows the maps of the averages values for February 2014 (Figure 4.1a) and the one obtained for September 2013 (Figure 4.1b). On February there are pixels without value, because, they are constantly covered by clouds.

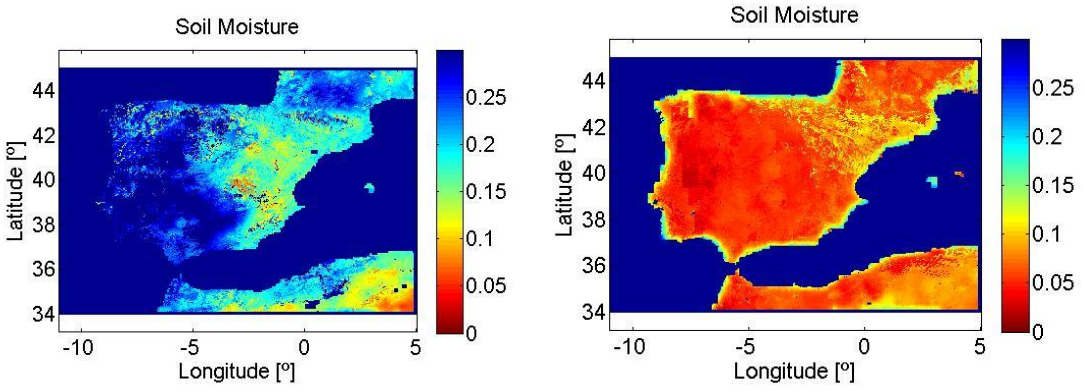

(a) (b)

Fig. 4.1: Soil moisture maps obtained averaging pixel values for a whole month. (a) February 2014 and (b) September 2013.

The map of February (Figure 4.1a) shows that even though the average of a complete month have been computed the problem of clouds still persists on some areas, especially on the South-western part of the peninsula. This problem may be even worst in other areas of the world, such as Northern Europe, because of their more cloudy weather. On the other side, the average map for September (Figure 4.1b), has values for all the pixels. September is a less cloudy month. Nevertheless, in this case some strange behaviors can be appreciated for some months and at some parts.

When this average value is used for filing the empty parts of the maps usually a strange behavior can be observed in the limiting area between measured values and interpolated values. Figures 4.2, 4.3 and 4.4 are examples of these effects.

4.2.2 Spatial interpolation

Linear interpolation has been applied to fill up gaps on high resolution soil moisture maps. A linear interpolation from values around the missing area are computed and used for filling the gaps. If the area to be filled up is quite small the interpolation gives quite satisfactory results. Nevertheless, when the area size increases strange artifacts are appreciated.

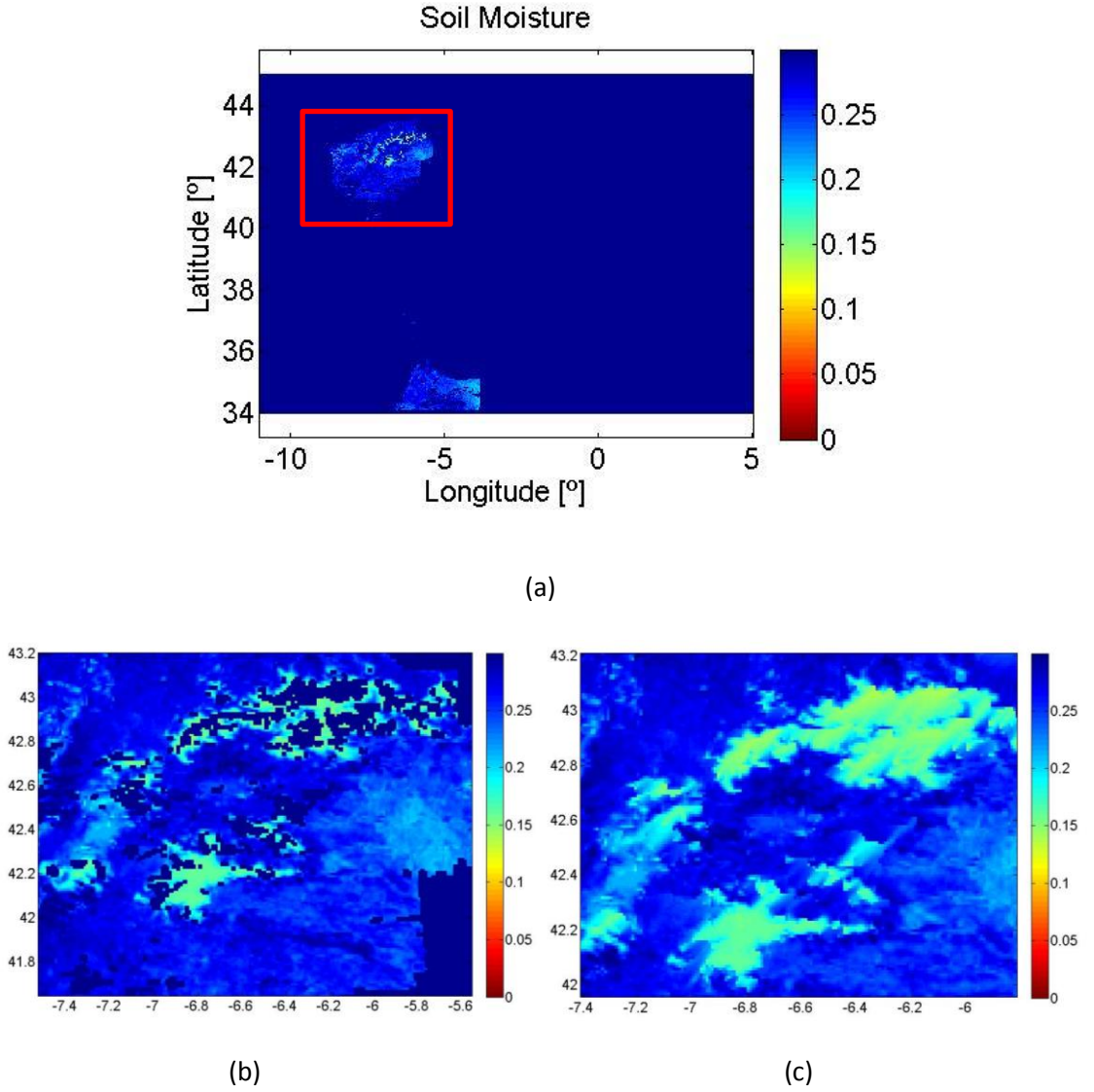

Fig. 4.2: (a) Soil moisture map from February the 27th, 2014 of the satellite pass on the western part of the Iberian Peninsula. (b) Zoom of the area framed in the picture (a). (c) Result of the linear interpolation of the same area.

Figure 4.2 demonstrate that this methodology may obtain good approximations for small areas to be filled up (figures 4.2b and 4.2c). However, it would be impossible to determine the value of larger cloudy areas in which not all the limiting values have been measured (for example Portugal gap in figure 4.2a) or even in cases where the area to be covered is too big.

4.2.3 Temporal interpolation

When spatial interpolation does not work properly a temporal interpolation could be used. In this case, the value for filling the gaps is obtained by interpolation of data from maps before and/or after the day of interest. In this case, large areas do not represent a big problem. But, during winter months some areas have no data for long periods and then, the temporal interpolation must be done from data quite far away on time, which can give not very accurate results.

Two different algorithms can be used:

- Filling up the values from maps of the closest days in time with values on the cloudy areas.
- Apply an interpolation function using the known values from days closer to the map to be filled up. A moving window (for example for a month long) can be used to obtain an interpolated function with data every day.

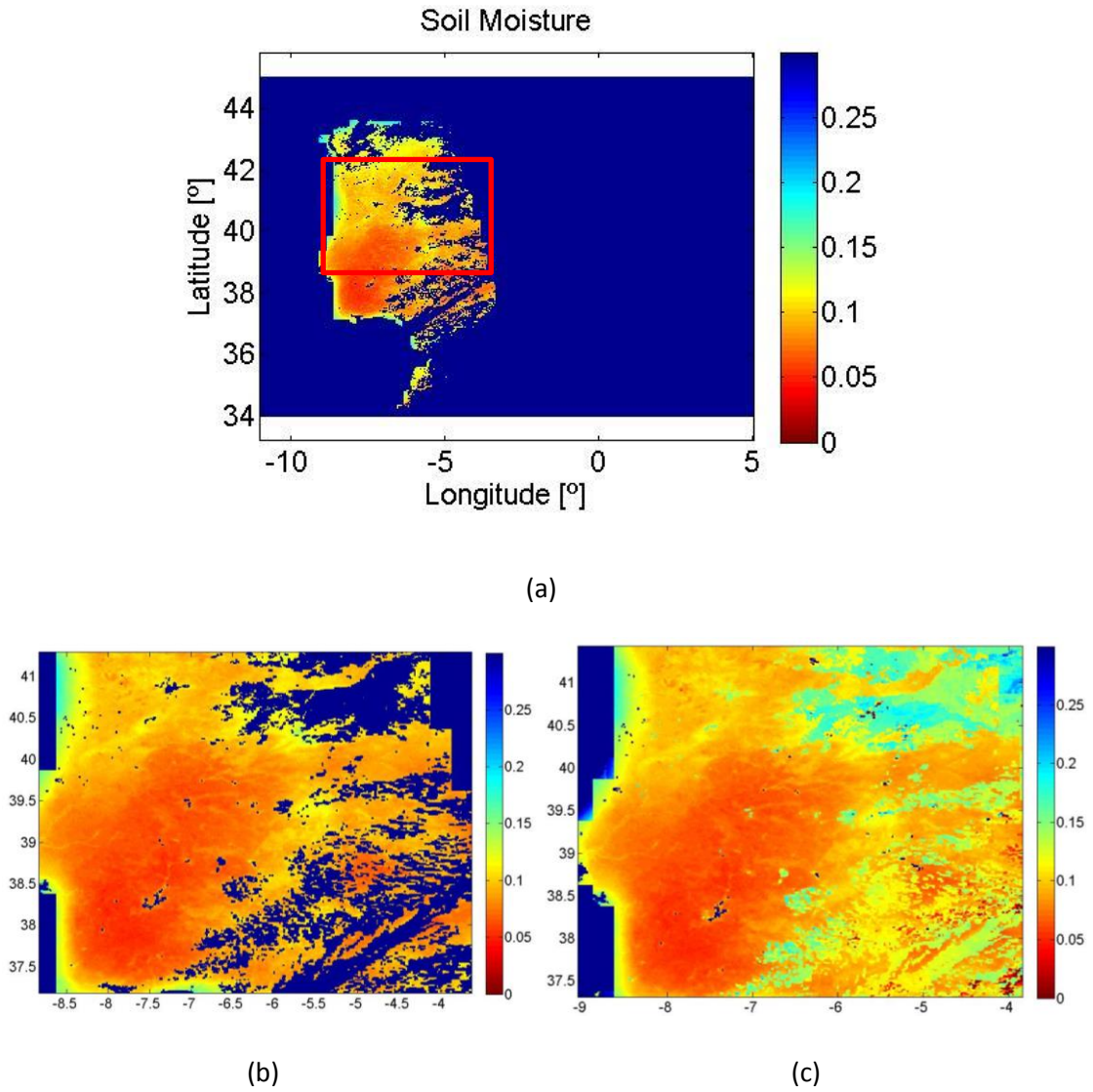

Fig. 4.3: (a) Soil moisture map from September the 8th, 2013 of the satellite pass on the western part of the Iberian Peninsula. (b) Zoom of the area framed in the picture (a). (c) Result of the temporal interpolation of the same area.

Figure 4.3, obtained by a linear interpolation using values from maps of the closest days, provides results that cannot be considered to be correct since it is quite unlikely that the areas affected by the presence of clouds have a value of soil moisture that is twice than those unaffected areas.

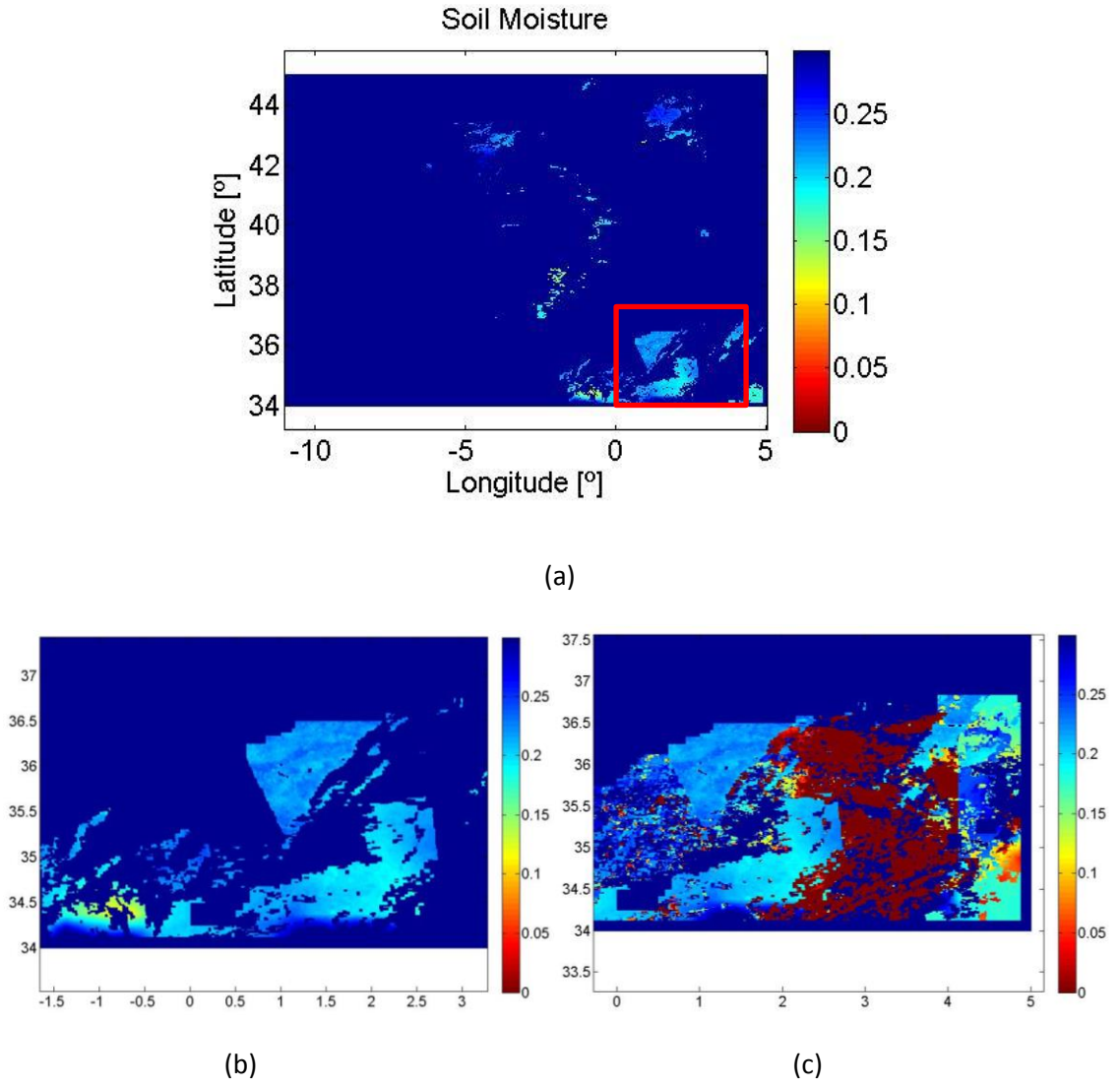

Fig. 4.4: (a) Soil moisture map from February the 8th, 2014 of the satellite pass on the eastern part of the Iberian Peninsula. (b)Zoom of the area framed in the picture (a). (c) Result of the temporal interpolation of the same area.

Figure 4.4 presents results obtained by a spline interpolation using the known values of maps closer to the map to be filled up. The results obtained in this case are worse than the previous one because the area that is filled with the new data have values that are far from the original ones. Besides, the problem of clouds is not solved as it happened in linear interpolations. It is important to know exactly the correct use of this kind of interpolations because the results obtained may strongly differ depending the number of days used. It can also affect if the day to be filled up is located in the center of the bunch of all the used days or it is in the beginning/ending and also, if there are too many days without data for computing the interpolation function. Then, the conclusion is that, spatial or temporal interpolation could be only be used on small areas and with only few days without data.

5. ALL WEATHER HIGH RESOLUTION MAPS USING ERA-INTERIM PRODUCTS

The results obtained using interpolations have not been satisfactory, so it was necessary the need to seek an alternative procedure to obtain high resolution soil moisture maps in all weather conditions, such as areas covered by clouds. The solution lies in using LST data from ERA-Interim dataset of ECMWF and combining them with the other variables already used in the downscaling algorithm (NDVI from MODIS).

5.1 ERA-INTERIM PRODUCTS

ERA-Interim (http://www.ecmwf.int/en/research/climate-reanalysis/era-interim) [23] is a global atmospheric reanalysis from 1979, continuously updated in real time. ERA-Interim data can be downloaded from the ECMWF (European Centre for Medium-Range Weather Forecasts). Public Datasets web interface or directly retrieved from MARS (class=ei, expver=1). Consult the ERA-Interim archive document (version 2) [34] for a full description of available parameters and diagnostic products. It provides a large range of weather variables such as soil moisture, wind speed or ice coverage. Its database is used as a substitute to LST. Two temperatures have been used in the development of this part of the project. Both present a spatial resolution of 12.5 km and are free of clouds:

- Skin temperature: It is the temperature referring to the Earth's surface.
- L1 temperature: It is the temperature that is obtained in a depth of 0-7cm below the Earth's surface.

Before selecting one of them, it has been performed a study of the behavior of applying the three following products: L1, Skin and an averaged value of both. This analysis was carried out all over the year 2013 by comparing results on areas where SMOS combined with LST from MODIS could provide data. Very similar results were appreciated, but, perhaps the best results were obtained using Skin temperature.

5.2 BEST ERA-INTERIM HOUR

ERA-Interim provides data four times a day: 00h, 06h, 12h and 18h. A study for selecting the best hour of data acquisition has been done for the year 2013. The conclusion was that 12h is the best hour, which is in agreement with a study already made by Miriam Pablos [35], which conclude that, the best surface temperature to be used in soil moisture retrievals with SMOS data is the daily maximum temperature, around midday. Table 5.1 presents the statistics (correlations R and root Mean Square errors) results when comparing in-situ measurements from REMEDHUS and the SM

retrievals when using LST from L1 ERA-interm, SKIN ERA-interim, an averaged value of the two of them or when using data from MODIS AQUA sensor.

	Morning			Afternoon			Morning	
	Average 06h	**Average 12h**	**AQUA 06h**	**Average 12h**	**Average 18h**	**AQUA 18h**	**L1 12h**	**SKIN 12h**
R	0.67	0.67	0.65	0.64	0.64	0.54	0.66	0.67
RMSE	0.11	0.11	0.10	0.12	0.12	0.10	0.11	0.11
RMSEc	0.07	0.07	0.06	0.08	0.08	0.06	0.08	0.07

Table 5.1: R and RMSE and RMSEc errors obtained using an average value of ERA-INTERIM SKIN AND L1 LSTs, with respect to the errors using AQUA MODIS LST at different hours. Also the errors obtained when directly using L1 and SKIN are presented.

In table 5.1, the comparison of the error obtained in Skin, LST, L1 and an average value of them at 6h, 12h and 18h, respect to values obtained when MODIS is used is presented. It can be seen data very similar results are obtained when using skin or an average temperature datasets. Consequently, it seems unnecessary to compute the average value and the Skin temperature have been selected. RMSE and RMSEc ERA-Interim errors suffer a slight increase respect of SMOS AQUA but correlation R improves

Once the best hour has been chosen, the study has been carried out for 5 years and it has been seen that the results improve the high resolution soil moisture maps as they provide maps almost full in the area compressed inside satellite passes. Another of the improvements is a better soil moisture detection in most of the terrains studied belonging to REMEDHUS area.

5.3 RESULTS AND VALIDATION

It has been demonstrated that Skin temperature from ERA-interim database can be used instead of LST from MODIS for obtaining high resolution maps. Using skin temperature from has two advantages: the accuracy is similar to the one obtained when using MODIS LST and it is not affected by weather conditions, such as cloudy days. Using the disaggregation method presented in chapter three and ERA-Interim database, new soil moisture maps have been obtained. All the results obtained have been compared, when it has been possible, with measures "in situ" taken inside the area of REMEDHUS and also with the measurements taken with SMOS in order to quantify the improvement that provides the use of ERA-Interim. In this section high resolution soil moisture maps free of clouds, using ERA-Interim Skin temperature in the disaggregation formula presented in chapter 3 are presented. The REMEDUS in-situ measurements for different soil types have been used for validation: annual comparisons of correlations and errors for different terrain types and a study for soil moisture maps free of clouds, annual comparisons of correlations and errors for different terrain types and a study for some special stations are presented.

5.3.1 Maps obtained with the new methodology

Examples of soil moisture maps that are obtained with surface temperature of ERA-interim skin dataset, combined with NDVI from MODIS; Brightness temperature at h and v polarization from SMOS and the downscaling algorithm presented in chapter 3 are used for computing the new soil moisture L4 product (see figure 5.2).

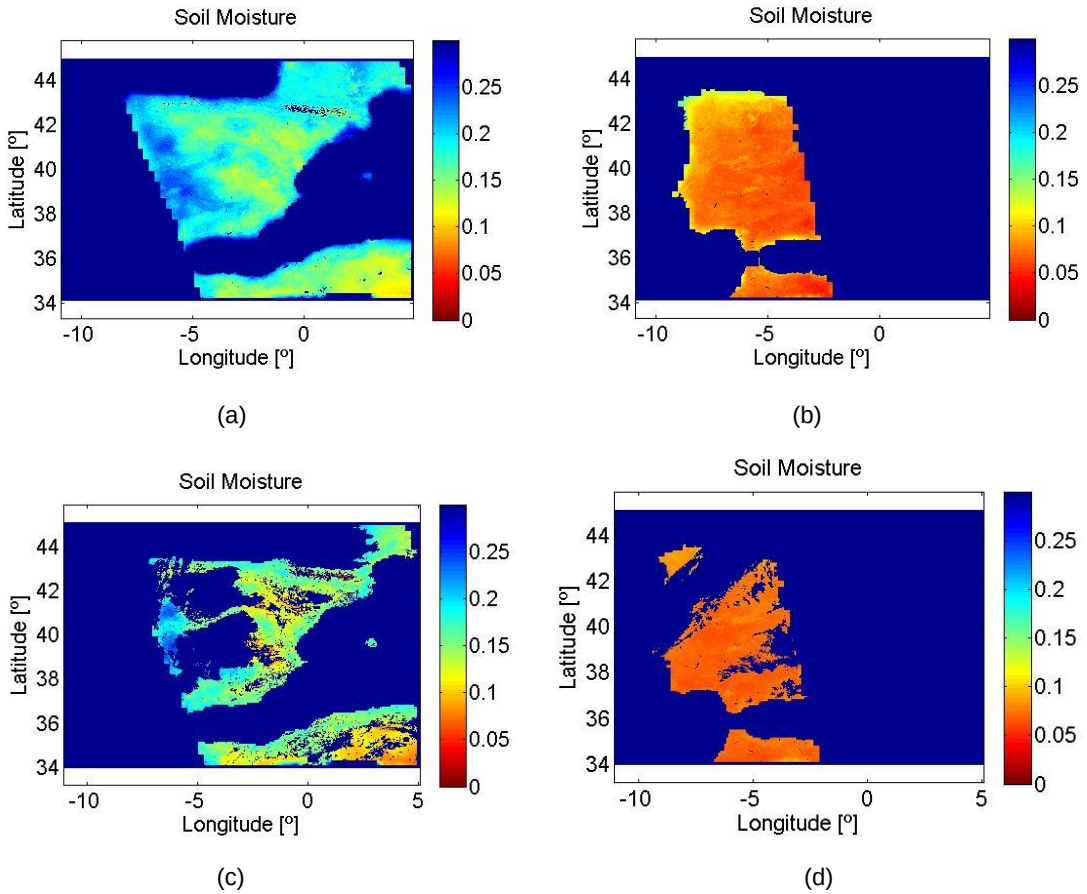

Fig. 5.2: (a) (b) Soil moisture maps from January the 8th and August the 16th, both from 2013, obtained with ERA-Interim. (c) (d) Soil moisture maps from the same days obtained with MODIS-AQUA

Figures 5.2 (a and b), provide filled maps in all the area measured by an SMOS overpass. Only few pixels affected by mountains or lakes, are empty. This maps contrast with the 5.2c) and d), that they have empty areas because of cloudy weather. Figure 5.3 shows for each pixel on the Iberian Peninsula, the number of days for the year 2012 with soil moisture high resolution data when using ERA-interim LST product or LST from MODIS. There are areas where few data per year can be retrieved when using LST MODIS, meanwhile when using ERA-interim they can be computed. Images in figure 5.4 present results obtained for the same study but for the year 2013.

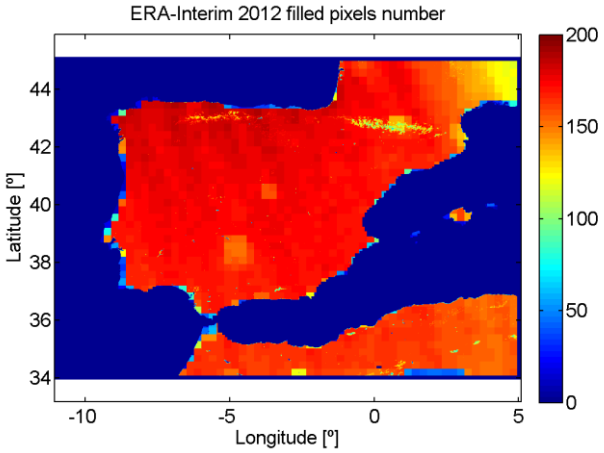

(a)

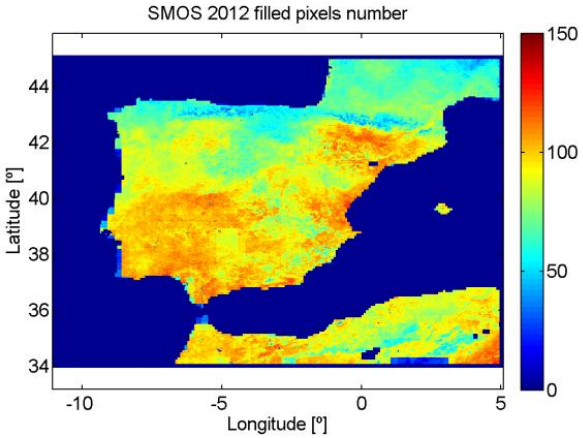

(b)

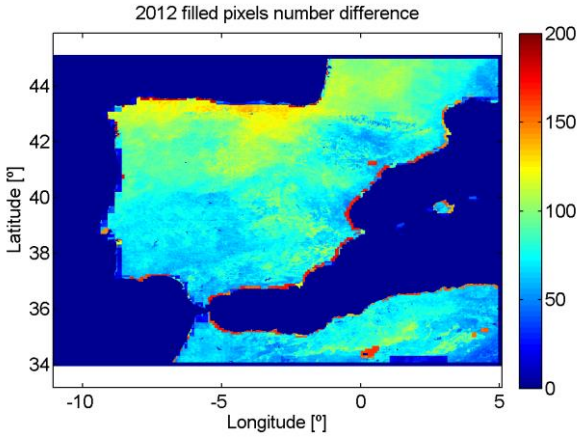

(c)

Fig. 5.3: (a) Number of days for each pixel with soil moisture high resolution data filled for the entire year 2012 when using LST temperature from ERA-Interim. (b) The same but for MODIS-AQUA. (c) Difference map

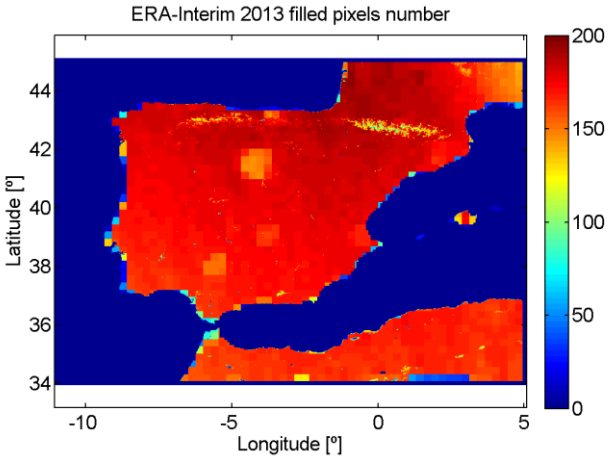

(a)

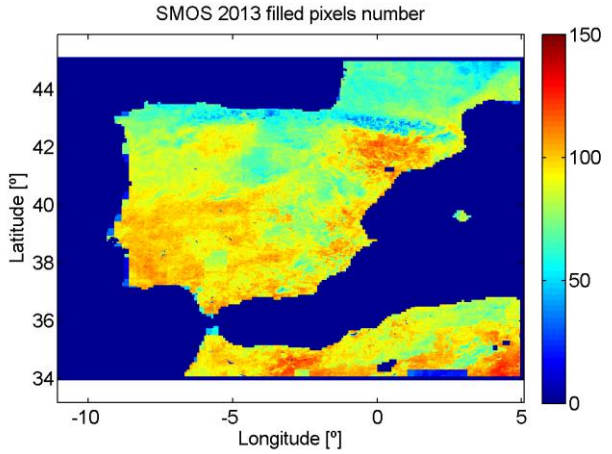

(b)

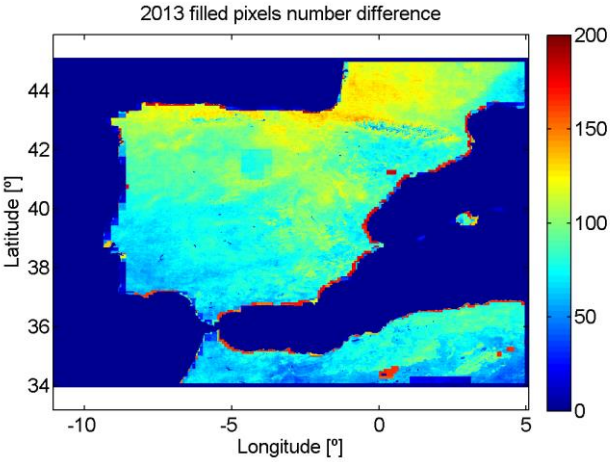

(c)

Fig. 5.3: (a) Number of days for each pixel with soil moisture high resolution data filled for the entire year 2013 when using LST temperature from ERA-Interim. (b) The same but for MODIS-AQUA. (c) Difference map

Taking into account the number of days of the year and the fact that satellite morning passes do not acquire data for the whole peninsula every day (a complete map is obtained every three days), it can be seen that when using this new approach (a) there are more than 160 days that have value for the same pixel in almost the whole surface. On the other hand, SMOS AQUA (b) has about 120 days in the best of cases. In the last row of the figures (c) it has been calculated the difference between ERA-Interim and SMOS AQUA. It is always positive because the new methodology brings more filled pixels. It should be pointed out that the Mediterranean coast gets filled pixels number values close to 190 and the northern part of the peninsula also looks benefited by ERA-Interim.

Next section is devoted to validate this new approach with in-situ REMETHUS measurements.

5.3.2 Validation of high resolution maps computed using ERA-Interim skin temperature respect to REMEDHUS in-situ measurements

The set of REMEDHUS stations is located in different types of terrain [see Annex-REMEDHUS Station Usage], which are *vineyard, forest-pasture, rainfed* and *fallow*. The same station may be associated to a specific terrain type within a specific year and the following year can be associated to another.

First of all, it has been observed the correlations between ERA-Interim, SMOS AQUA and measures "in situ". To do this, the averages of daily soil moisture data [2] obtained in the area of REMEDHUS have been used and have been contrasted with the one obtained via satellite. In addition, root mean square errors (RMSE and RMSEc (centered)) have been computed. Best results have been obtained for years 2012 and they are presented in figure 5.5.

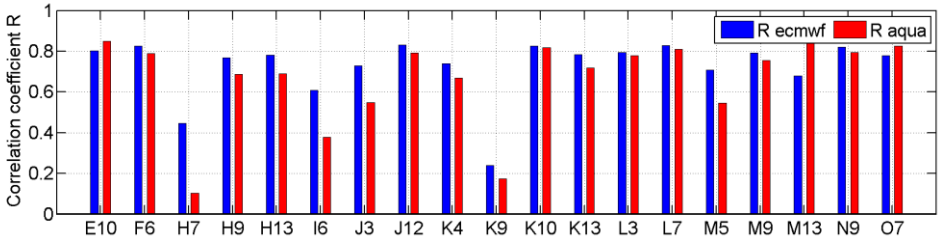

(a)

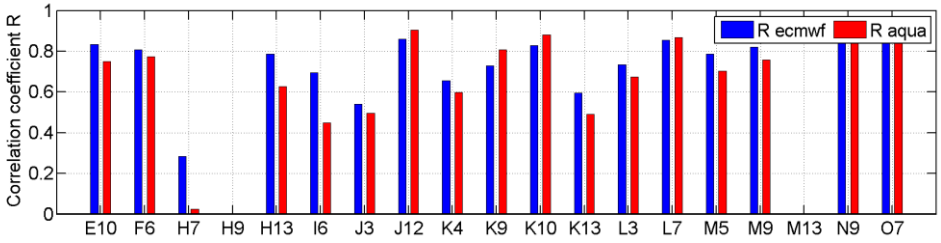

(b)

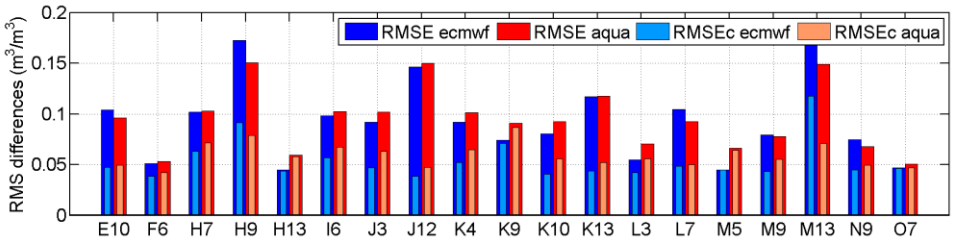

(c)

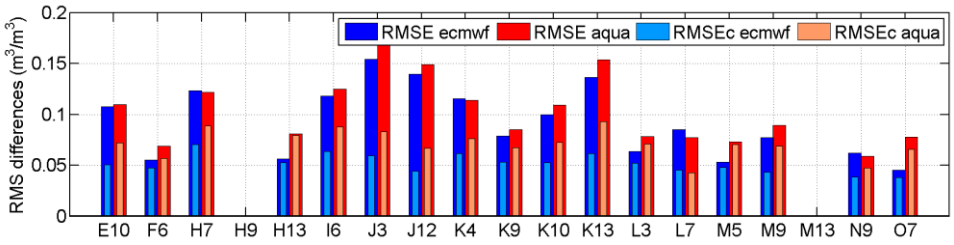

(d)

Fig. 5.5: Annual correlations (a) (b) and errors (c) (d) between ERA-Interim ECMWF and MODIS-AQUA for each REMEDHUS station in years 2012 and 2013

In figure 5.5, it can be seen the improvement in detection that carries out the new methodology. With the exception of some specific stations as O7, there is a greater correlation when using ERA-Interim data than using MODIS-AQUA. In addition to this, it should be noted that the station H7, which is *vineyard* in all five years and is located in an extremely dry spot. Then the soil moisture retrieval is less in agreement than in other areas. K9 is irrigated in the year 2012, which complicates the acquisition of data. In the same way, the error is usually less in ERA-Interim than in MODIS-AQUA with the exception of the H9 and M13, the two *forest-pasture* stations. This type of terrain is difficult to detect with ERA-Interim because for all years MODIS-AQUA gives better results. Furthermore, these two stations are located on the bottom of valleys and therefore are easier to suffer floods. For year 2013 there is no data for these two stations. It should be remarked also that RMSEc is almost always around 5%, which is the desirable situation.

Year 2011, shown in figure 5.6, presents results that are opposite to what happens in years 2012 and 2013:

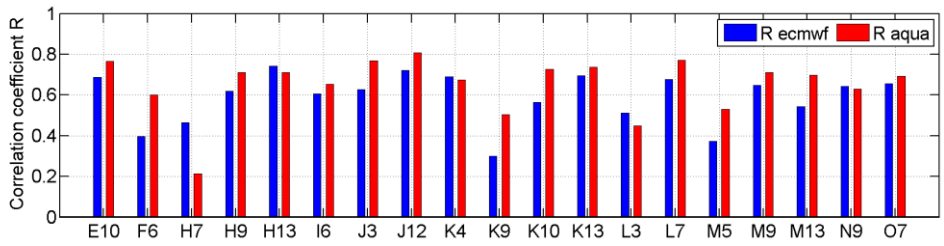

(a)

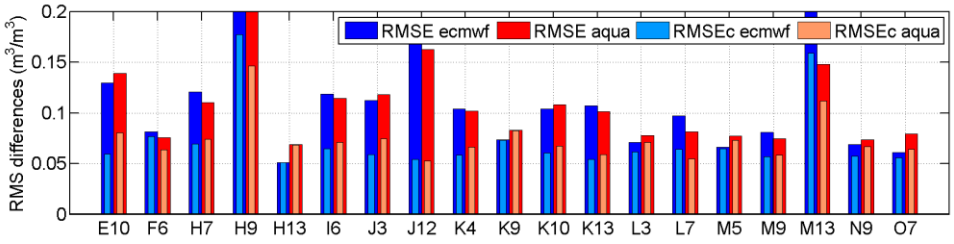

(b)

Fig. 5.6: Annual correlations (a) and errors (b) between ERA-Interim ECMWF and MODIS-AQUA for each REMEDHUS station in year 2011

This figure serves to illustrate the worst year in terms of results obtained. As it can be seen, MODIS-AQUA has a better correlation and its error tends to be lower in most cases. As in year 2012, station K9 is also irrigated. The detection of fallow stations H13 and J12 is quite similar but different for station M5. Also it is noteworthy the big error in *forest-pasture* (H9 and M13) as well as in station J12. This last station suffered a change from being *rainfed* in 2010 to become *fallow* in 2011. This can be a reason for having this unexpected error value.

The rest of years, 2010 and 2014, presented similar results between the two methods globally. For year 2010 it is necessary to comment that there is an initial period of six months, of which there are very few data due to satellite tuning and by year 2014 there is only data from *forest-pasture* belonging to one station H9.

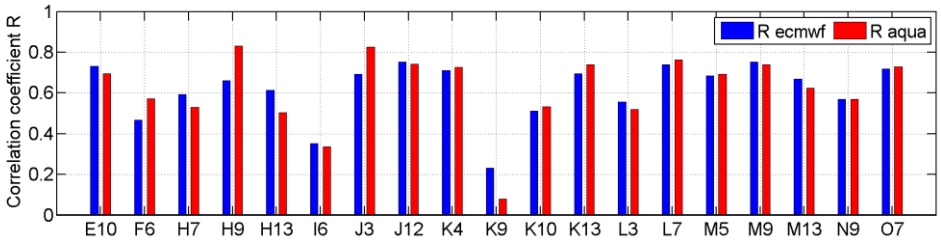

(a)

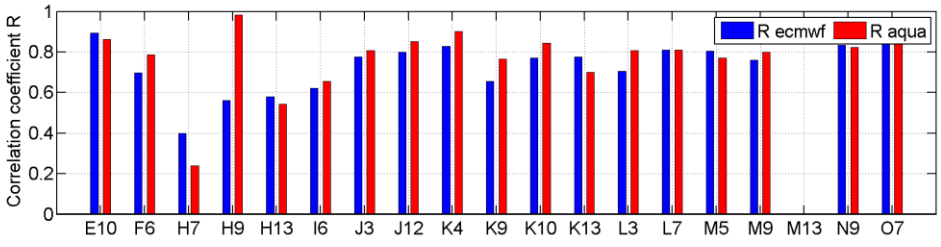

(b)

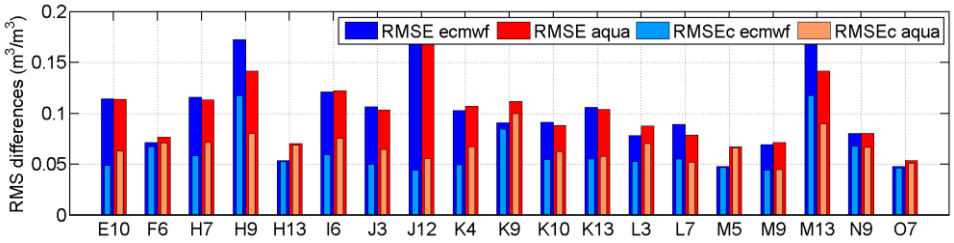

(c)

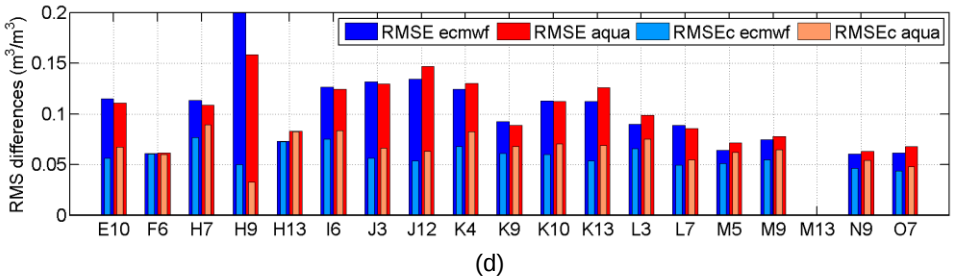

(d)

Fig. 5.7: Annual correlations (a) (b) and errors (c) (d) between ERA-Interim ECMWF and MODIS-AQUA for each REMEDHUS station in years 2010 and 2014

In figure 5.7, it can be seen that practically the two methods are very similar. Leaving aside the problems associated with stations H9, J12, K9 and M13 as commented in other years, the remaining stations have equivalent correlation and error results.

As a collection, the total correlation average for each terrain type as well as the associated errors can be found in table 5.2. Only the annual results are shown:

	2010		2011		2012		2013		2014	
	Era-Interim	SMOS	Era-Interim	SMOS	Era-Interim	SMOS	Era-Interim	SMOS	Era-Interim	SMOS
Vineyard										
R	0.59	0.60	0.56	0.59	0.70	0.57	0.65	0.53	0.68	0.69
RMSE	0.10	0.10	0.10	0.11	0.08	0.09	0.10	0.11	0.11	0.11
RMSEc	0.06	0.07	0.06	0.07	0.05	0.06	0.06	0.08	0.07	0.07
Rainfed										
R	0.69	0.70	0.65	0.71	0.80	0.78	0.80	0.80	0.79	0.82
RMSE	0.10	0.10	0.09	0.09	0.09	0.09	0.09	0.09	0.08	0.08
RMSEc	0.05	0.05	0.06	0.06	0.04	0.05	0.05	0.06	0.05	0.06
Forest-Pasture										
R	0.66	0.73	0.58	0.70	0.72	0.77	-	-	0.56	0.98
RMSE	0.18	0.14	0.25	0.19	0.18	0.15	-	-	0.23	0.16
RMSEc	0.12	0.09	0.17	0.13	0.10	0.07	-	-	0.05	0.03
Fallow										
R	0.65	0.63	0.61	0.68	0.78	0.69	0.75	0.65	0.75	0.75
RMSE	0.07	0.07	0.10	0.10	0.08	0.08	0.08	0.10	0.11	0.12
RMSEc	0.06	0.06	0.06	0.06	0.04	0.06	0.05	0.08	0.06	0.07
Total										
R	0.62	0.62	0.58	0.65	0.73	0.66	0.74	0.68	0.73	0.77
RMSE	0.10	0.10	0.11	0.11	0.09	0.09	0.09	0.10	0.10	0.10
RMSEc	0.06	0.07	0.07	0.07	0.05	0.06	0.05	0.07	0.06	0.07

Table 5.2: Average correlations for each terrain type and associated errors for all of the years studied

In table 5.2 it can be extracted that for *vineyard* terrain type the new methodology provides a great improvement in years 2012 and 2013 or it remains similar for the other years. The same happens for *fallow* terrain types. In the case of *rainfed* terrain types, the two methodologies have very similar results. Finally, for *forest-pasture* terrains MODIS-AQUA detects soil moisture much better than ERA-Interim. Regarding to the errors, there is no situation in which ERA-Interim is above of MODIS-AQUA except for *forest-pasture* terrain types, where it is greater. Anyway, in the latter case the error is

also large for MODIS-AQUA and it can be concluded that this terrain type is difficult to detect for both methodologies.

5.3.3 Regression slopes: Comparison between ERA-Interim and SMOS in different REMEDHUS stations

Scatter plots displaying the agreement between remotely sensed data and REMEDHUS in situ measurements with segments illustrating the linear fit of seasonal data have been obtained. Results are shown for representative stations. They reflect the all-weather product has a higher number of estimates and its slope of the linear correlation is improved. In the following figures several examples of the graphics as well as the slopes for the regression lines are shown both for SMOS and for ERA-Interim: (Annex has all of the stations for all of the studied years)

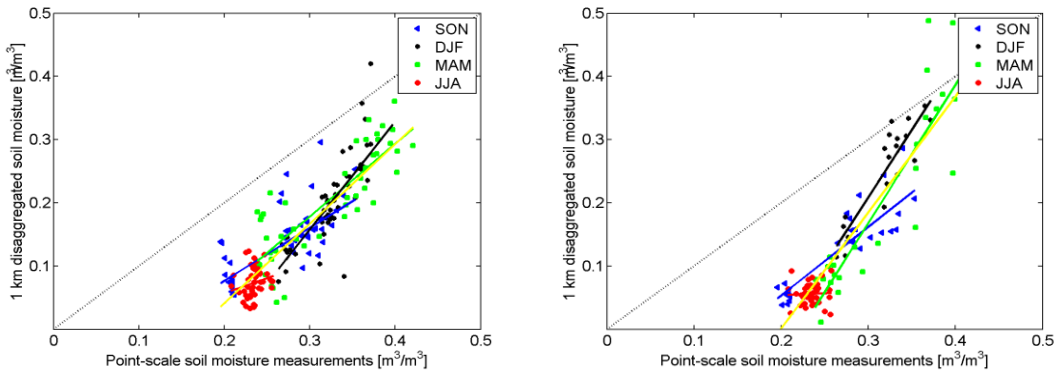

(a) (b)

Fig. 5.8: Regression line slopes for the station J12 in 2013. Rainfed terrain type. (a) ERA-Interim and (b) SMOS AQUA. View of all seasons of the year: SON (September-October-November), DJF (December-January-February), MAM (March-April-May) and JJA (June-July-August)

	Station J12	
	ERA-Interim	**SMOS AQUA**
Summer (red)	0.4667	0.0577
Autumn (blue)	0.8405	1.0861
Spring (green)	1.1503	2.1865
Winter (black)	1.7065	2.1291
All (yellow)	1.2584	1.8338

Table 5.3: Comparison between regression line slopes for station J12

In figure 5.8, with the exception of autumn, which has a regression line slope closer to 1 in SMOS AQUA, ERA-Interim presents more accurate slopes. Furthermore, it should be noted also the presence of a greater number of points in the case of ERA-Interim result of having maps free of clouds. The slope for all of the seasons, in yellow, shows clearly that the new methodology provides an improvement as a whole.

The summer shows difficulties in their detection because there is a tendency to have very dry areas in the region of REMEDHUS by that time of the year. The high values for soil moisture samples in SMOS AQUA during spring have to be noticed. The reason for that may be that in year 2013 there was a situation of extreme humidity in the Duero

river area, according to the Resumen Mensual Climatológico [36] of the Ministerio de Agricultura, Alimentación y Medio Ambiente.

Another example, in this case of *vineyard* terrain type for year 2012, is found in figure 5.9:

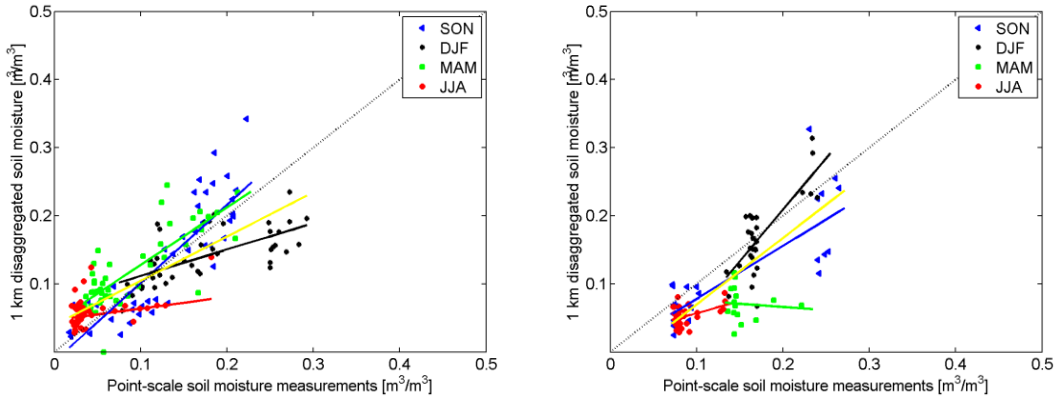

(a) (b)

Fig. 5.9: Regression line slopes for the station F6 in 2012. Vineyard terrain type. (a) ERA-Interim and (b) SMOS AQUA. View of all seasons of the year: SON (September-October-November), DJF (December-January-February), MAM (March-April-May) and JJA (June-July-August)

	Station F6	
	ERA-Interim	**SMOS AQUA**
Summer (red)	0.2641	0.3493
Autumn (blue)	1.2414	0.7795
Spring (green)	0.9222	-0.0920
Winter (black)	0.8448	1.5094
All (yellow)	0.9130	0.9768

Table 5.4: Comparison between regression line slopes for station F6

The station F6 serves to illustrate that, while the regression slope line for all of the stations has a better result for SMOS AQUA, this is due to the low amount of data points. The spring is best detected by ERA-Interim and autumn is almost in the ideal case. It should be noted also that SMOS AQUA, as well as in the previous case, tends to assign lower soil moisture values to the pixels than the assigned by the new methodology; that's why the points positions are moved slightly to the right.

Returning to the case of *rainfed* terrain type stations, which are the most common, figure 5.10 provides another example of it:

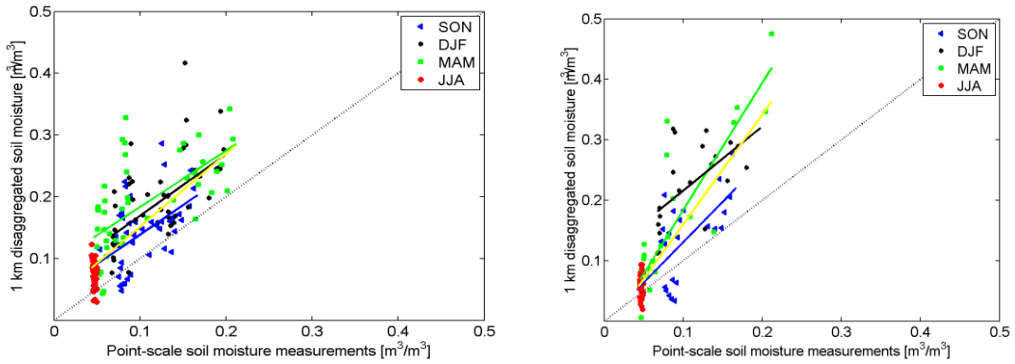

(a) (b)

Fig. 5.10: Regression line slopes for the station K9 in 2013. Rainfed terrain type. (a) ERA-Interim and (b) SMOS AQUA. View of all seasons of the year: SON (September-October-November), DJF (December-January-February), MAM (March-April-May) and JJA (June-July-August)

	Station K9	
	ERA-Interim	**SMOS AQUA**
Summer (red)	-4.6740	-1.4947
Autumn (blue)	0.9555	1.3401
Spring (green)	0.9123	2.1016
Winter (black)	0.9925	1.0611
All (yellow)	1.1836	1.8162

Table 5.5: Comparison between regression line slopes for station K9

In figure 5.10 it can be found once more the problem of detection during the summer. The regression line slopes that is obtained for this season is not characteristics since the distribution of points is too vertical. For the rest of the stations the slopes are very close to 1.

The last case is set in a fallow terrain type, in this case for year 2014. Figure 5.11 serves as an example to illustrate again that more points provide more accuracy:

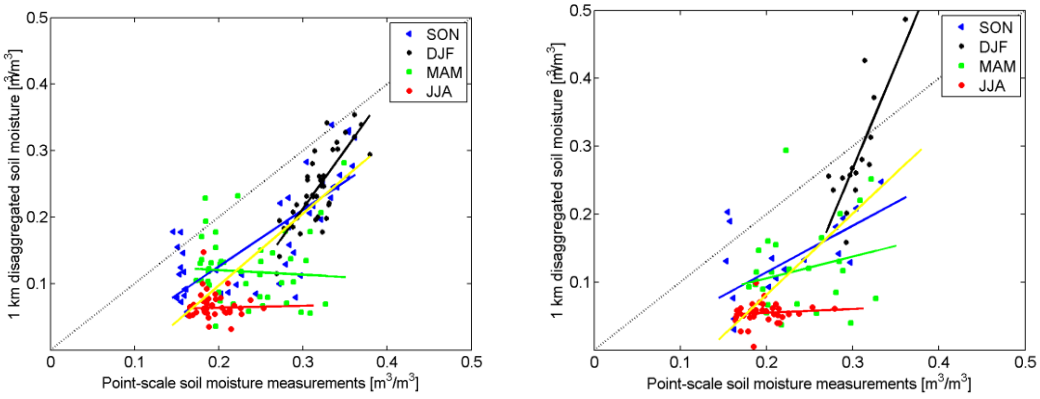

(a) (b)

Fig. 5.11: Regression line slopes for the station K13 in 2014. Fallow terrain type. (a) ERA-Interim and (b) SMOS AQUA. View of all seasons of the year: SON (September-October-November), DJF (December-January-February), MAM (March-April-May) and JJA (June-July-August)

	Station K13	
	ERA-Interim	**SMOS AQUA**
Summer (red)	0.0272	0.0574
Autumn (blue)	0.8521	0.6836
Spring (green)	-0.0689	0.3193
Winter (black)	1.7608	3.0401
All (yellow)	1.0839	1.1926

Table 5.6: Comparison between regression line slopes for station K13

In this case, it can be verified that a greater distribution of points can also serve to correct a situation that is believed favorable. For example, the spring for SMOS AQUA has a positive slope, while for ERA-Interim, having more points, shows that the trend is actually to go down. As in other cases, ERA-Interim is better than SMOS-AQUA as a whole.

This evaluation study supports the use of the all-weather version since it does not depend on cloud cover and the accuracy of the estimates with respect to in-situ data in improved or preserved. However, there are certain days of the year in which the maps obtained show zones that do not have the resolution of 1 km. These days feature spacious areas with the same soil moisture values for all of the pixels included in them. A more detailed analysis of these maps and the procedure studied in order to learn the cause of this problem can be found in the following subchapter.

5.4 LOW RESOLUTION ERA-INTERIM SOIL MOISTURE MAPS

For every year, there is a small amount of days that present low resolution problems. These days are not adapted to high resolution and have zones that remain at low resolution. The number of problematic days has been obtained, temporarily for a first approach, by means of a threshold for the a_3 coefficient, which accompanies NDVI. The threshold is set at values greater than 0.005 and lower to 0.005. Any day with a value of a_3 coefficient between these values has been considered problematic. As examples of these days, figure 5.12 shows two characteristic maps for them.

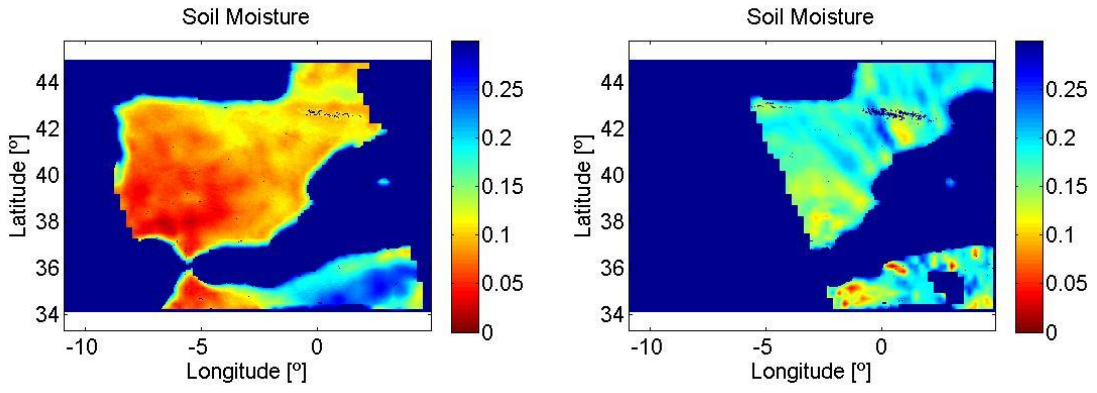

(a) (b)

Fig. 5.12: Soil moisture maps for (a) June the 3th and (b) December the 26th. The maps present areas which are not adapted to high resolution.

The total number of days that are affected by this problem separated in years is shown in table 5.7:

	Total number of valid days	Number of problematic days
2010	249	26
2011	334	24
2012	334	18
2013	352	18
2014	340	18

Table 5.7: Number of problematic days of all of the total number of days

In order to understand why this happens, various factors that take part in the process of changing from low resolution to high resolution are considered. In particular, it has been studied the value of the medians of the coefficients a_n for each of the elements of the equation 5.1, the value of the diagonal matrix coefficients solved by the least squares procedure, the number of observations in low resolution for each problematic day in order to see if it affects only a few days or many days and chi-square error for every day in order to quantify if problematic days feature a very high error.

5.4.1 Coefficients medians

In the coefficients case, the value has been obtained for all days of the year, for problematic days and for all not problematic days. The days that are affected are distributed throughout the year, so it cannot be determined if it only affects a single season or a specific period of time. In the Annex, the tables for all coefficients can be found; in this chapter only LST and NDVI coefficients medians are shown because they are the ones who have the most anomalous results. Tables 5.8 and 5.9 refer to these two coefficients respectively.

	a_2 (LST)					
	Problematic		**Not problematic**		**All**	
	Absolute value	**Without absolute**	**Absolute value**	**Without absolute**	**Absolute value**	**Without absolute**
2010	0.0457	-0.0249	0.0381	-0.0089	0.0566	-0.0110
2011	0.0377	- 0.0090	0.0413	-0.0198	0.0498	-0.0192
2012	0.0538	-0.0360	0.0481	-0.0187	0.0420	-0.0193
2013	0.0746	-0.0532	0.0493	-0.0339	0.0532	-0.0361
2014	0.0428	-0.0254	0.0518	-0.0315	0.0497	-0.0309

Table 5.8: LST coefficient medians

	a_3 (NDVI)					
	Problematic		Not problematic		All	
	Absolute value	Without absolute	Absolute value	Without absolute	Absolute value	Without absolute
2010	0.0025	-0.0013	0.0381	0.0093	0.0344	0.0057
2011	0.0025	-0.0008	0.0413	0.0215	0.0383	0.0176
2012	0.0022	-0.0002	0.0481	0.0325	0.0451	0.0290
2013	0.0032	0.0009	0.0493	0.0362	0.0465	0.0333
2014	0.0025	0.0001	0.0518	0.0458	0.0493	0.0413

Table 5.9: NDVI coefficient medians

The median has been obtained both in absolute value and without it in order to see the corresponding weights as a whole. In LST case it can be seen that for problematic days, when making the median without the absolute value, the values that are obtained are quite different than those that are obtained throughout the year as a whole or only the days considered not problematic. LST is not provided at 1 km resolution, but values do not differ in excess of the total value. The same happens, to a more extreme, in the case of NDVI coefficient. The median goes to the fourth decimal in order to have a value different from 0. Compared to the total of the year, the values obtained for problematic days are really low. For the other coefficients [Annex-Coefficient Medians], the values obtained in all cases are similar and therefore have not been analyzed in more detail.

As mentioned in the methodology of this chapter, NDVI is also one of the elements that gives high resolution to the resulting soil moisture maps. Therefore, if the coefficient associated to it has a very low value, its function will be greatly affected in comparison to other factors and probably high resolution will not be reached.

5.4.2 Matrix coefficient diagonalization by the method of least squares

To continue with the study of the coefficients, it has been obtained also a graphic with the values of the matrix coefficients diagonalization. This procedure has been carried out for both days correct and for problematic days to see if there was any anomaly.

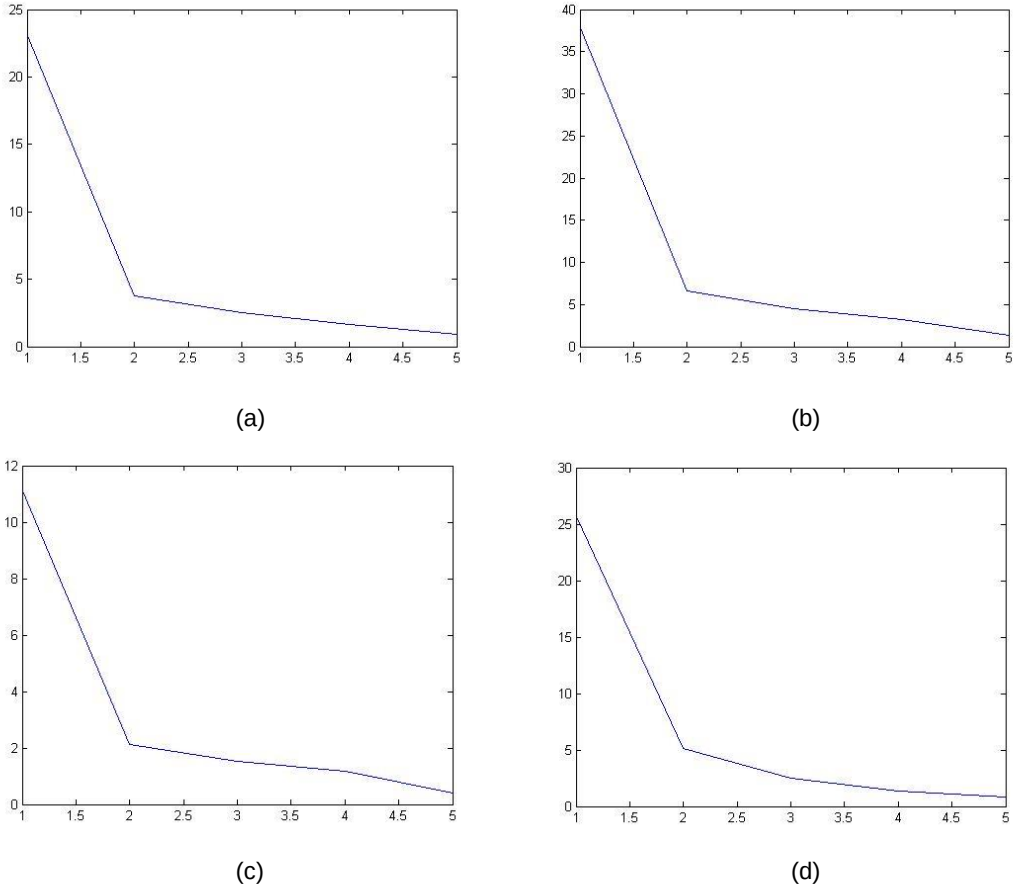

Fig. 5.13: (a) (b) Graphs showing the values of matrix coefficients diagonalization elements. (c) (d) The same but for problematic days.

In figure 5.13 it can be seen that there is no big difference between problematic and not problematic days. In the same way it has also been observed the dimension of this matrix for different values of tolerances. In any case it has been retrieved any value different from dimension five, which corresponds to the five coefficients a_n. For this reason, this is not considered as a factor which takes part in low resolution problematic days

5.4.3 Number of observations

At this point, it can be considered that the cause of this problem is the coefficient a_3. However, a study concerning the number of observations in low resolution in order to see if the problem affects only days with very few data has been made. If that was the case, these days could be eliminated, but as it will be shown, the problem affects a variety of days.

Continuing with the possible solutions, the number of observations in low resolution for every day of the year has been calculated. Table 5.10 shows the number of observation for all of the five years.

	Nobs < 200		Nobs > 200 Nobs < 400		Nobs > 400 Nobs < 600		Nobs > 600 Nobs < 800		Nobs > 800 Nobs < 10000		Nobs > 1000	
	All	**Probl**	**All**	**Probl**	**All**	**Probl**	**All**	**Probl**	**All**	**Probl**	**All**	**Probl**
2010	54	6	64	7	50	7	37	5	16	1	1	0
2011	50	3	77	7	57	3	60	7	38	4	27	0
2012	79	5	63	1	51	4	48	3	42	4	33	1
2013	54	6	66	4	47	4	63	1	66	2	38	1
2014	37	5	68	3	58	1	61	6	51	2	45	1

Table 5.10: Number of observations in low resolution for every day of the year

As it can be seen, the case of a number of observations less than 200 refers to satellite passes at the edge of the studied region. In this range there are a certain number of problematic days that cannot represent the whole number of these days. Specifically, the bulk of problematic days is set between 200 and 800 observations, which is equivalent to soil moisture maps moderately full. For this reason, these maps cannot be discarded because it would mean eliminating characteristic and useful data of the peninsula.

5.4.4 Chi-square error

The last of the tests in order to discern what the cause of this anomaly remained in observing values of the chi-square error medians for every problematic day, not problematic day and for the whole year. Table 5.11 shows the results:

	CHISQ2		
	Problematic	**Not problematic**	**All**
2010	0.00036	0.00037	0.00037
2011	0.00031	0.00045	0.00044
2012	0.00032	0.00037	0.00037
2013	0.00024	0.00056	0.00055
2014	0.00041	0.00054	0.00053

Table 5.11: Chi square error median values

In the same way that has happened for coefficient a_2 (LST), the results for problematic days are slightly lower than the values for the whole year. However, they are not as drastic as in the case of a_3 (NDVI) to be considered to be the source of the error.

5.4.5 Solution to problematic days

Observing the results presented by the study on the coefficients, the number of observations and the chi-square error, the solution that has been considered better to solve the soil moisture maps that present areas at low resolution is making a new graph of NDVI. In this graph it is represented the detection probability and false alarm probability. Trying different thresholds of NDVI, it has been retrieved the number of problematic days detected and the number of good days detected. Comparing these

days with those which have been considered problematic in a subjective way, it has come to the conclusion that the best is the threshold of NDVI between -0.02 and 0.02.

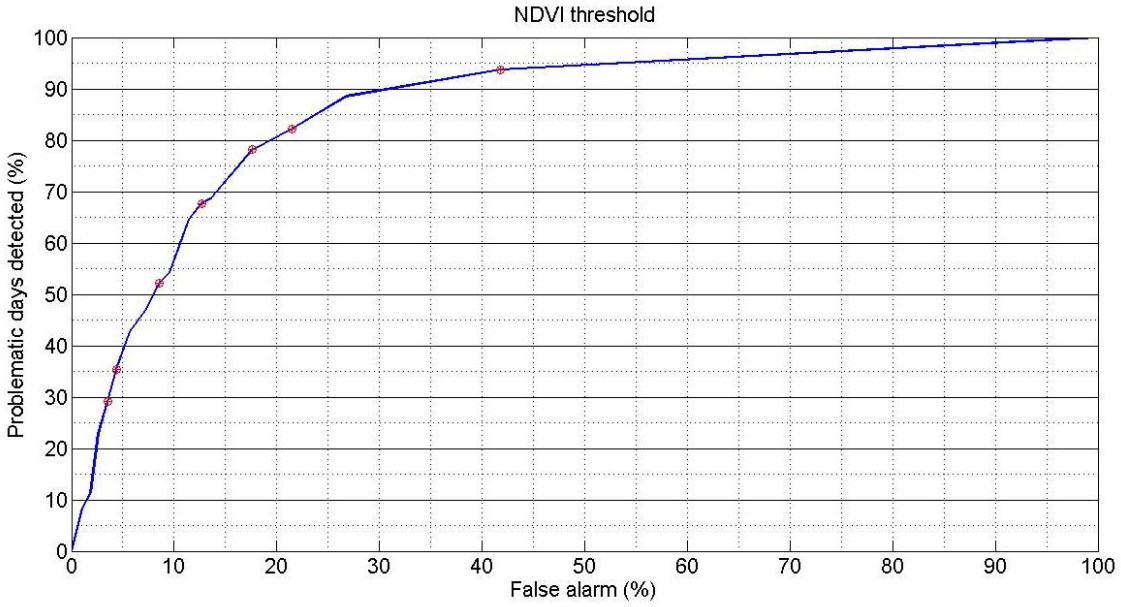

Fig. 5.14: Problematic day detection and false alarm for different thresholds

	NDVI threshold				
	-0.001, 0.001	**-0.002, 0.002**	**-0.003, 0.003**	**-0.004, 0.004**	**-0.005, 0.005**
False alarm	1.07	1.88	2.63	3.51	4.39
Detection	8.33	11.46	22.92	29.17	35.42
	-0.006, 0.006	**-0.007, 0.007**	**-0.008, 0.008**	**-0.009, 0.009**	**-0.010, 0.010**
False alarm	5.65	7.21	8.53	9.54	10.48
Detection	42.71	46.88	52.08	54.17	59.38
	-0.011, 0.011	**-0.012, 0.012**	**-0.013, 0.013**	**-0.016, 0.016**	**-0.020, 0.020**
False alarm	11.42	12.67	13.61	17.63	21.51
Detection	64.58	67.71	68.75	78.13	82.29
	-0.025, 0.025	**-0.040, 0.040**			
False alarm	26.79	41.78			
Detection	88.54	93.75			

Table 5.12: Different NDVI threshold probabilities

The red points in figure 5.14 correspond to NDVI steps of 0.004. The last one corresponds to NDVI -0.04, 0.04. NDVI -0.02, 0.02 has been considered the best because it detects 82.29 % of problematic days. The days detected will not be provided because they would not be used. However, 21.52 % of not problematic days will be lost. Taking into account that the total number of not problematic days is 1594 for the five years, that percentage means that 343 days will be lost. Referring to problematic days, 79 days of 96 subjectively detected will be detected, so only 17 problematic days remain in the products that will be provided.

After using the thresholds, the solution to the problematic days has been achieved and the new methodology has been considered really useful to solve the problems of the clouds.

6. CONCLUSIONS

The main objective of this project was to obtain high resolution maps in al weather conditions. The first version for improving the SM resolution maps retrieved by SMOS (50km) used high resolution data (1km) from MODIS. The two variables were LST and NDVI 1km resolution. Nevertheless, this sensor works at infrared and near-infrared band which are affected by weather conditions such as clouds and at cloudy conditions was impossible to obtain high resolution maps.

Some interpolation techniques for obtaining high resolution maps in cloudy conditions were studied without satisfactory results. Consequently, LST from ERA-interim dataset (ECMWF product) has been used with much better results: inter-comparison between data from the model and REMEDHUS in-situ measurements confirmed that correlations and RMS errors were preserved or even improved.

The satisfactory conclusions of this study have derived in the distribution of a new data at the SMOS-BEC. Soil moisture at fine-scale (BEC L4 soil moisture product) can now be estimated under all-weather conditions. A delayed 5-year (2010-2015) data set covering the Iberian Peninsula is already available, and maps from 2015 onwards are provided in near real-time. The L4 product is obtained by combining SMOS brightness temperatures with higher spatial resolution MODIS information into fine-scale soil moisture estimates [1,2]. In the new L4 version 3.0 or “all-weather” product, we are including ERA-Interim temperature in the downscaling algorithm, which allows fine-scale soil moisture mapping from space independently of cloud cover.

See figure 6.1 for an example of its application over Europe on July 1, 2014 (ascending passes). The version SMOS L4 is also provided (figure 6.2) to illustrate the differences between the two versions.

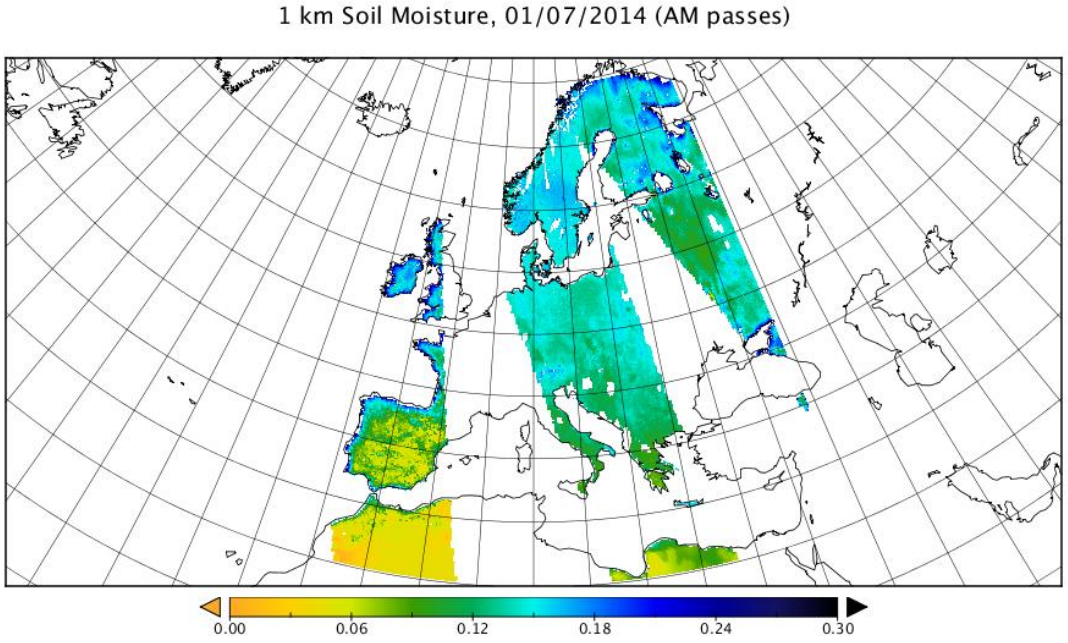

Fig. 6.1: All-weather 1 km soil moisture map at European scale for July the 1st, 2014. [SMOS BEC [37]]

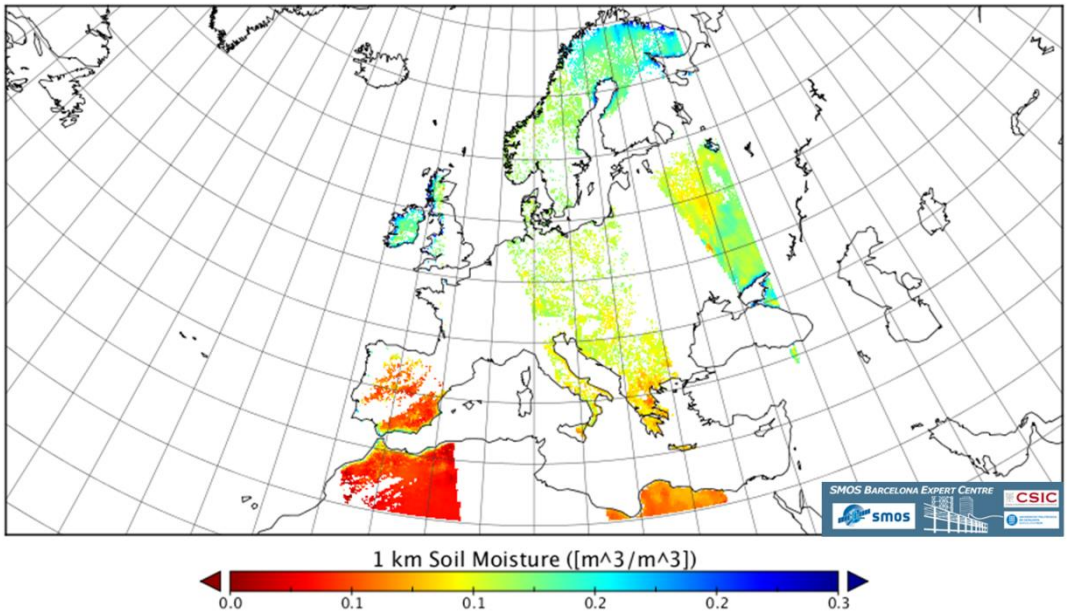

Fig. 6.2: SMOS L4 1 km soil moisture map at European scale for July the 1st, 2014. [SMOS BEC [37]]

6.1 FURTHER RESEARCH

As future line with the L4 all-weather product, it is planned to extend the downscaling approach to other climatic regions.

Furthermore, the combination of SMOS with other satellite sensors such as SEVERI, with 3km of resolution and data every 12minutes, can be studies. In this case, the maps are affected by clouds but as so many maps are obtained every day, the probability to have some maps per day without clouds is very high. A study of using an averaged map or the best map along the day could be really interesting.

On the other hand, Sentinel 2 has been recently launched, and synergies with its datasets are also recommended.

ACKNOWLEDGEMENT

I would like to thank the following people implied in the development of this project. Without each one of them, this project would never have ended.

First, to my family. All of them have been patient and have helped me in a lot of different ways.

Second, to UPC group. Special thanks to Mercè, María, Adriano, Gerard, Míriam and David for giving me such valuables advices and guiding me all this time.

Finally, to SMOS BEC, University of Salamanca and ERA-Interim for allowing me to use their datasets.

BIBLIOGRAPHY

[1] –Piles, M., Sanchez, N., Vall-llossera, M., Camps, A., Martinez Fernandez, J., Martinez, J., Gonzalez-Gambau et al. “A downscaling approach for smos land observations: evaluation of high resolution soil moisture maps over the Iberian Peninsula”. 2014.

[2] – Universidad de Salamanca. “Hydraprobe_REMEDHUS_2010-2015”. Excel documents containing soil moisture averages.

[3] – Peak W.H. “Interaction of Electromagnetic Waves with some natural surfaces”. IRE Transaction A.P. 7. 1959

[4] – Ulaby et al. “Microwave Remote Sensing”, vol I. Ed. Artech House 1981.

[5] – Image available at:

[http://image.slidesharecdn.com/antennabasics-130220062256-phpapp01/95/antenna-basics-4-638.jpg]

[6] –Piles, M. “Multiscale soil moisture retrievals from microwave remote sensing observations”. 2010

[7] – Ulaby et al. “Microwave Remote Sensing”, vol III. Ed. Artech House 1986.

[8] – Choudhury, B, Schmugge, T., Chang, A. and Newton, R. “Effect of surface roughness on the microwave emission from soils”, 1979.

[9] – Newton, R. and Rouse, J. “Microwave radiometer measurements of soil moisture content” 1980.

[10] – Wang, J. and Choudhury, B. “Remote sensing of soil moisture content over bare field at 1.4 GHz frequency”. 1981.

[11] – Wigneron, J., Laguerre, J. and Kerr, Y. “A simple parameterization of the L-band microwave emission from rough agricultural soils”. 2001.

[12] – Mo, T., Choudhury, B. and Schmugge, T. “A model for microwave emission from vegetation-covered fields”. 1982.

[13] – van der Griend, A. and Wigneron, J. “The b-factor as a function of frequency and canopy type at H-polarization”, 2004.

[14] – Burke, E., Shuttleworth, W. and French, N. “Using vegetation indices for soil moisture retrievals from passive microwave radiometry”, 2001.

[15] – EUROPEAN SPACE AGENCY. SMOS, la misión del agua de la ESA. Resumen de la misión [date of consultation: 05/15/2015]. Available at:

[http://www.esa.int/esl/ESA_in_your_country/Spain/SMOS_-_La_Mision_del_agua_de_la_ESA_-_Resumen_de_la_mision_Factsheet]

[16] – EUROPEAN SPACE AGENCY. MIRAS, A Two-Dimensional Aperture-Synthesis Radiometer for Soil-Moisture and Ocean-Salinity Observations [date of consultation: 05/15/2015]. Available at:

[http://www.esa.int/esapub/bulletin/bullet92/b92marti.htm]

[17] – Zundo, M., Barré, H. and Hahne, A. “SMOS product definition baseline SO-TN-ESA-GS-1250”, 2005.

[18] – SMOS Barcelona Expert Center. Image available at:

[http://www.smos-bec.icm.csic.es/sites/www.smos-bec.icm.csic.es/files/smos_final_new.jpg]

[19] – EOPORTAL DIRECTORY. Aqua Mission (EOS/PM-1) [date of consultation: 05/15/2015]. Available at:

[https://directory.eoportal.org/web/eoportal/satellite-missions/a/aqua]

[20] – NASA. AQUA Earth-observing satellite mission [date of consultation: 05/15/2015]. Available at:

[http://aqua.nasa.gov/]

[21] – NASA. MODIS Moderate Resolution Imaging Spectroradiometer [date of consultation: 05/15/2015]. Available at:

[http://modis.gsfc.nasa.gov/about/specifications.php]

[22] – NASA. Image available at:

[http://eoimages.gsfc.nasa.gov/images/imagerecords/2000/2421/aqua_deploy.1.jpg]

[23] – ECMWF. ERA-Interim [date of consultation: 05/15/2015]. Available at:

[http://www.ecmwf.int/en/forecasts/datasets/era-interim-dataset-january-1979-present]

[http://www.ecmwf.int/en/research/climate-reanalysis/era-interim]

[24] – ECMWF. ERA-Interim, Daily

[http://apps.ecmwf.int/datasets/data/interim-full-daily/]

[25] – C. Conesa García, J.B. Martínez Guevara et al. “Territorio y Medio Ambiente. Métodos Cuantitativos y Técnicas de Información Geográfica”. Ed. Universidad de Murcia 2004. Pages: 182-184

[26] – MDPI. Review of the CALIMAS Team Contributions to European Space Agency’s Soil Moisture and Ocean Salinity Mission Calibration and Validation. [date of consultation: 04/28/2015]. Image available at:

[http://www.mdpi.com/remotesensing/remotesensing-04-01272/article_deploy/html/images/remotesensing-04-01272f11-1024.png]

[27] – Wigneron, J., Calvet, J., Pellarin, T, van der Griend, A., Berger, M. and Ferrazzoli, P. “Retrieving near-surface soil moisture from microwave radiometric observations: current status and future plans. 2003.

[28] – Frate, F. D., Ferrazzoli, P. and Schiavon, G. “Retrieving Soil moisture and agricultural variables by microwave radiometry using neural networks”. 2003.

[29] – SMOS Barcelona Expert Center. Available at:

[http://www.smos-bec.icm.csic.es/smos_bec]

[30] – SMOS Barcelona Expert Center. SMOS BEC Team. [date of consultation: 03/10/2015]. Pages: 13-17. Available at:

[http://cp34-bec.cmima.csic.es/doc/BEC-SMOS-0001-PD.pdf]

[31] – LP DAAC (NASA & USGS). MODIS/Aqua Land Surface Temperature and Emissivity Daily L3 Global 1km Grid SIN MYD11A1. [date of consultation: 05/15/2015].. Available at:

[https://lpdaac.usgs.gov/products/modis_products_table/myd11a1]

[32] – LP DAAC (NASA & USGS). Vegetation Indices 16-Day L3 Global 1km MOD13A2. [date of consultation: 05/15/2015].. Available at:

[https://lpdaac.usgs.gov/products/modis_products_table/mod13a2]

[33] – Solano, R., Didano, K., Jacobson, A. and Huete, A. "MODIS Vegetation Index User's Guide (MOD13 Series)". 2010.

[34] – Berrisford, P., D. Dee, P. Poli, R. Brugge, K. Fielding, M. Fuentes, P. Kallberg, S. Kobayashi, S. Uppala and A. Simmons. "The ERA-Interim archive Version 2". 2011

[35] –Pablos, M., Piles, M., Sánchez-Martín, N., González-Gambau, V., Vall-llossera, M., Camps, A. and Martínez, J. "A sensitivity study of land surface temperature to soil moisture using in-situ and spaceborne observations". IGARRS 2014

[36] - Ministerio de Agricultura, Alimentación y Medio Ambiente. Gobierno de España. "Resumen Mensual Climatológico. Marzo de 2013". 2013.

[37] – Piles, M., Pou, X., Camps, A., Vall-Llossera, M. and SMOS Barcelona Expert Center Team. SMOS BEC. [date of consultation: 05/20/2015]. Available at:

[http://cp34-bec.cmima.csic.es/doc/BEC-SMOS-L4SMv3-QR.pdf]

ANNEXES

REMEDHUS STATION USAGE

STATION	2010	2011	2012	2013	2014
E10	V	V	V	V	V
11	R	R	F	R	F
F6	V	V	V	V	V
H13	F	F	F	F	F
H7	V	V	V	V	V
H9	F-P	F-P	F-P	F-P	F-P
I6	V	V	V	V	V
J12	R	F	R	R	F
J14	R	R	F	R	R
J3	V	V	V	V	V
K10	R	R	R	R	R
K13	R	R	F	F	I
K4	V	V	R	R	F
K9	I	I	I	R	R
L3	V	V	V	V	V
L7	F	R	F	R	R
M13	F-P	F-P	F-P	F-P	F-P
M5	F	F	F	R	R
M9	R	R	R	R	R
N9	F	R	R	R	R
O7	R	R	R	F	R
21X				R	R

V: vineyard

R: rainfed

F: fallow

F-P: forest-pasture

I: irrigated

REGRESSION LINES

From left to right and up to down, years 2010 to 2014 if not specified the contrary.

E10 STATION

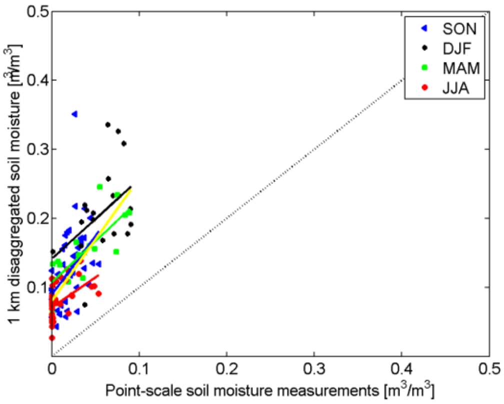

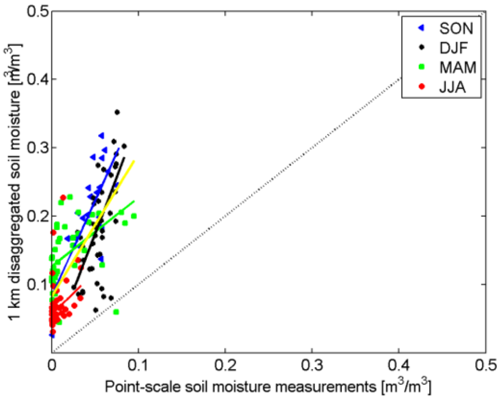

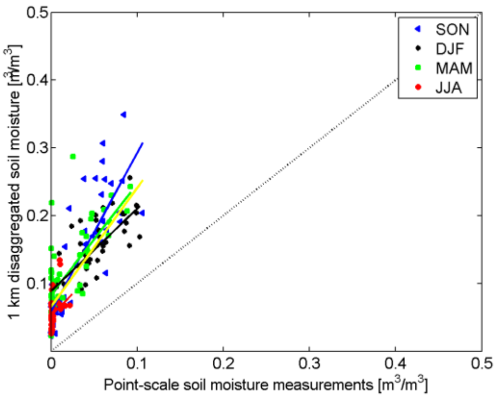

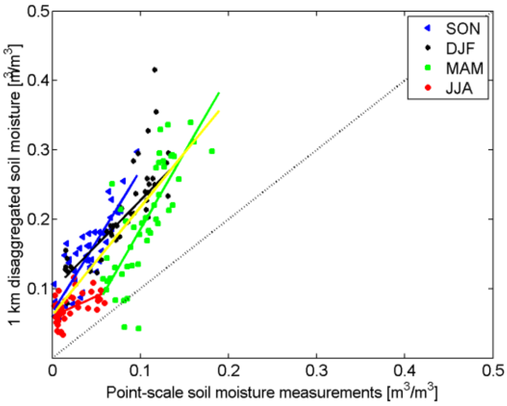

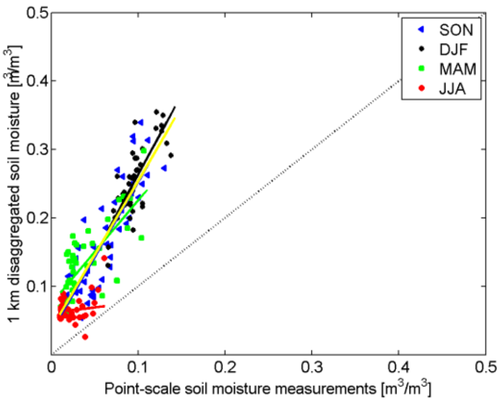

F6 STATION

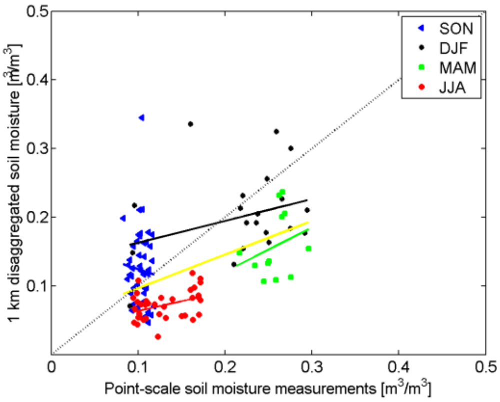
SON
DJF
MAM
JJA
1 km disaggregated soil moisture [m3/m3]
Point-scale soil moisture measurements [m3/m3]

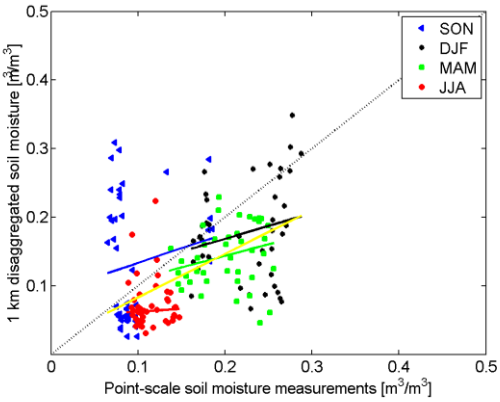
SON
DJF
MAM
JJA
1 km disaggregated soil moisture [m3/m3]
Point-scale soil moisture measurements [m3/m3]

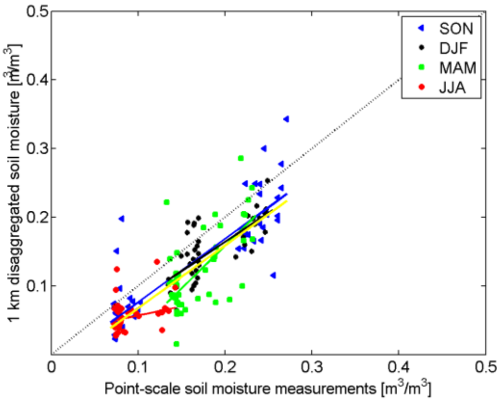
SON
DJF
MAM
JJA
1 km disaggregated soil moisture [m3/m3]
Point-scale soil moisture measurements [m3/m3]

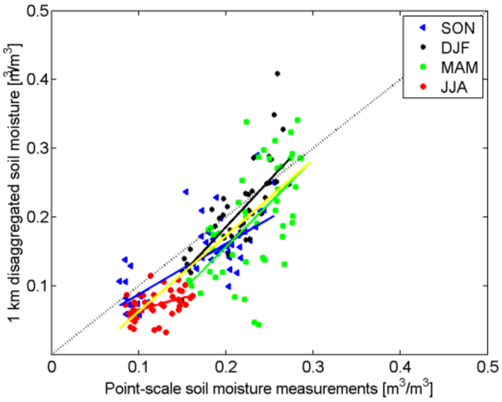
SON
DJF
MAM
JJA
1 km disaggregated soil moisture [m3/m3]
Point-scale soil moisture measurements [m3/m3]

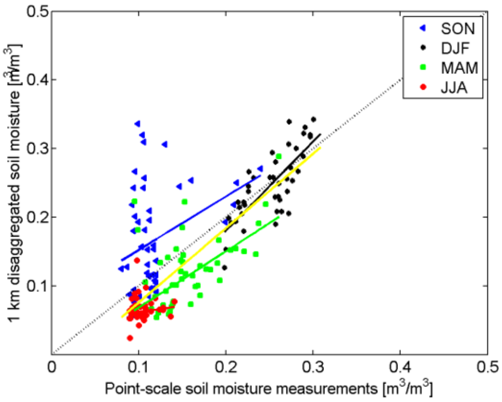
SON
DJF
MAM
JJA
1 km disaggregated soil moisture [m3/m3]
Point-scale soil moisture measurements [m3/m3]

H7 STATION

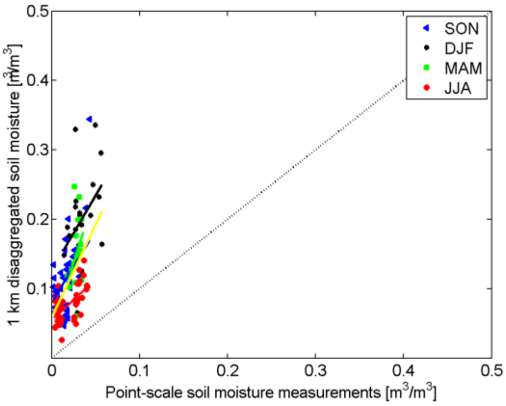
SON
DJF
MAM
JJA
1 km disaggregated soil moisture [m3/m3]
Point-scale soil moisture measurements [m3/m3]

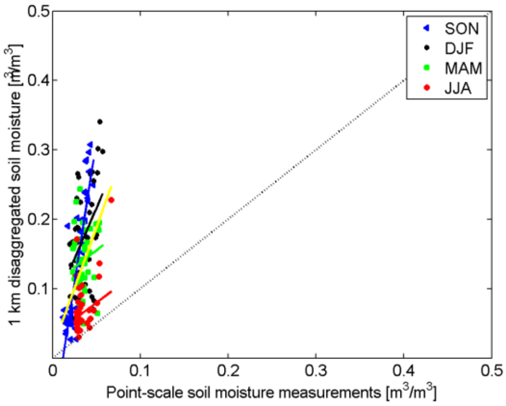
SON
DJF
MAM
JJA
1 km disaggregated soil moisture [m3/m3]
Point-scale soil moisture measurements [m3/m3]

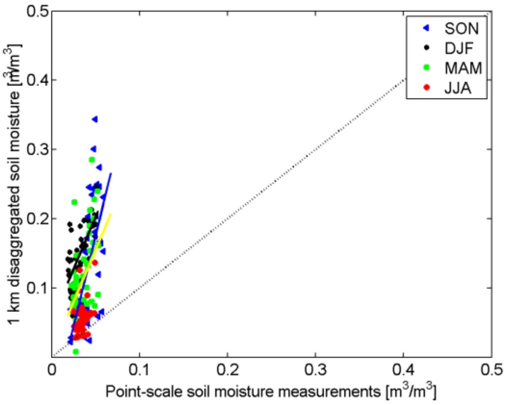
SON
DJF
MAM
JJA
1 km disaggregated soil moisture [m3/m3]
Point-scale soil moisture measurements [m3/m3]

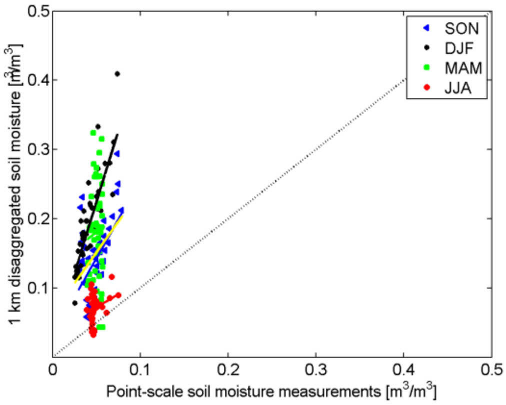
SON
DJF
MAM
JJA
1 km disaggregated soil moisture [m3/m3]
Point-scale soil moisture measurements [m3/m3]

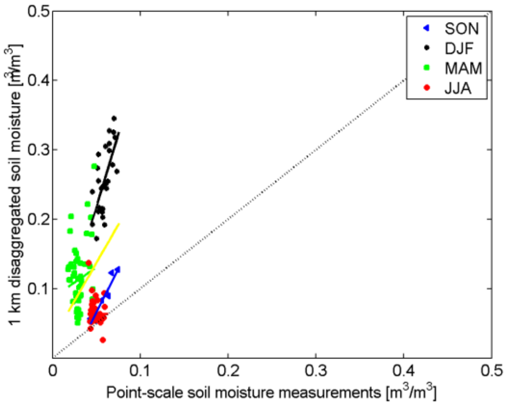
SON
DJF
MAM
JJA
1 km disaggregated soil moisture [m3/m3]
Point-scale soil moisture measurements [m3/m3]

H9 STATION

Year 2013 and 2014 do not have data, so last image belongs to year 2012.

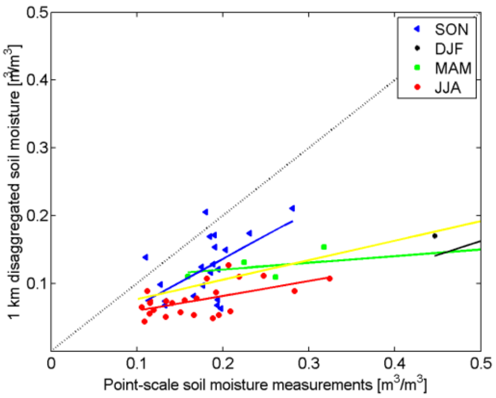

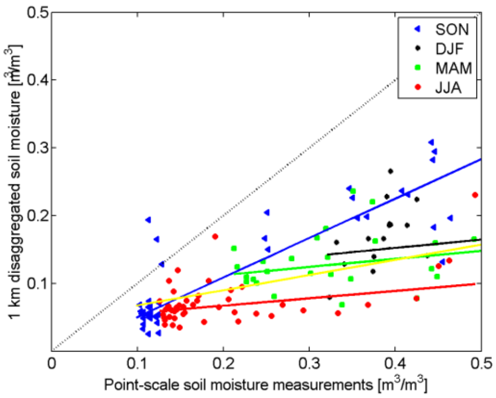

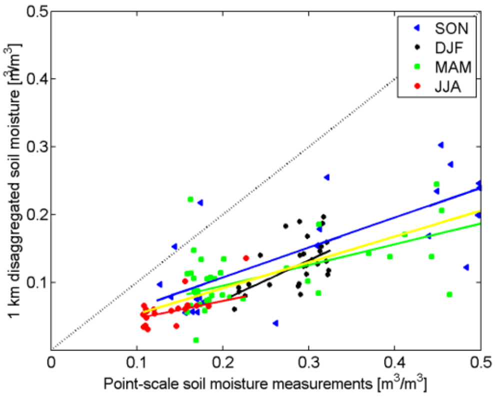

H13 STATION

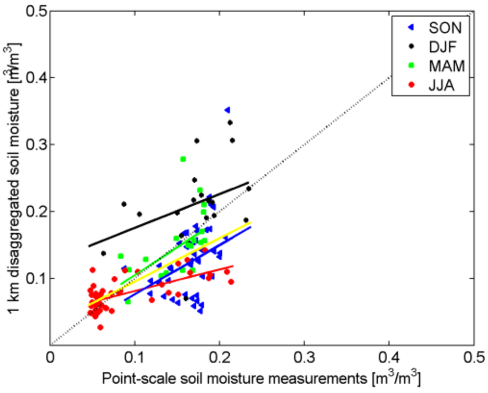
SON
DJF
MAM
JJA
1 km disaggregated soil moisture [m3/m3]
Point-scale soil moisture measurements [m3/m3]
0
0.1
0.2
0.3
0.4
0.5

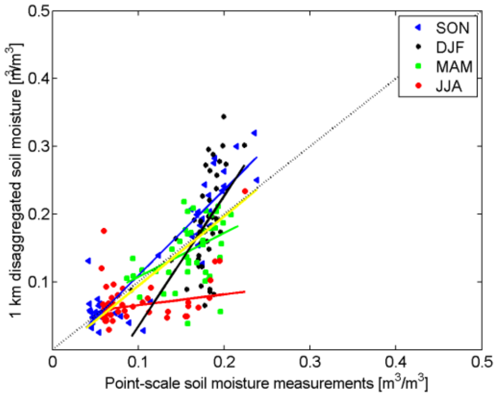
SON
DJF
MAM
JJA
1 km disaggregated soil moisture [m3/m3]
Point-scale soil moisture measurements [m3/m3]
0
0.1
0.2
0.3
0.4
0.5

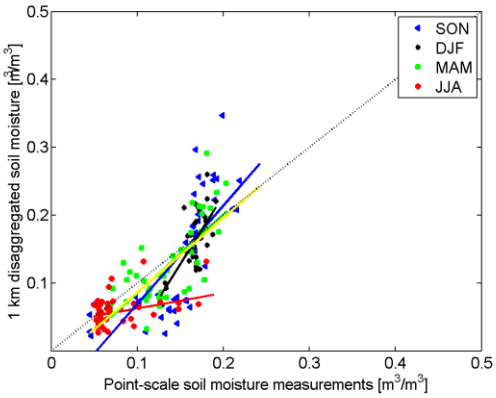
SON
DJF
MAM
JJA
1 km disaggregated soil moisture [m3/m3]
Point-scale soil moisture measurements [m3/m3]
0
0.1
0.2
0.3
0.4
0.5

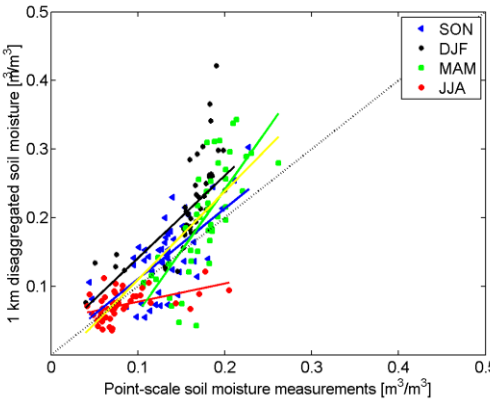
SON
DJF
MAM
JJA
1 km disaggregated soil moisture [m3/m3]
Point-scale soil moisture measurements [m3/m3]
0
0.1
0.2
0.3
0.4
0.5

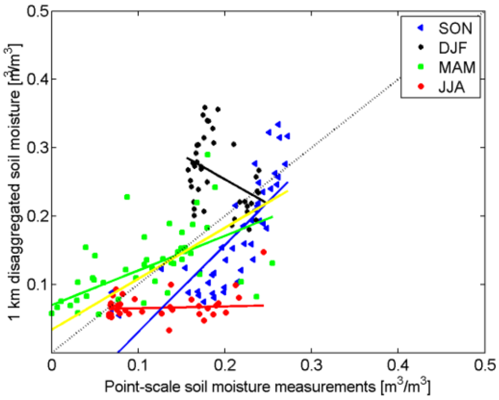
SON
DJF
MAM
JJA
1 km disaggregated soil moisture [m3/m3]
Point-scale soil moisture measurements [m3/m3]
0
0.1
0.2
0.3
0.4
0.5

I6 STATION

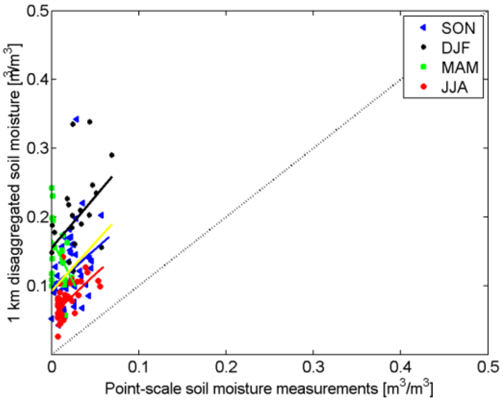

SON
DJF
MAM
JJA
1 km disaggregated soil moisture [m3/m3]
Point-scale soil moisture measurements [m3/m3]

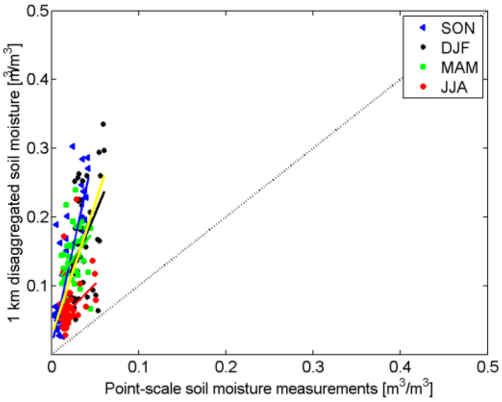

SON
DJF
MAM
JJA
1 km disaggregated soil moisture [m3/m3]
Point-scale soil moisture measurements [m3/m3]

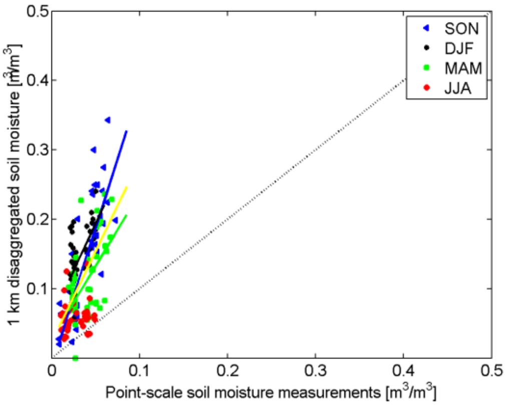

SON
DJF
MAM
JJA
1 km disaggregated soil moisture [m3/m3]
Point-scale soil moisture measurements [m3/m3]

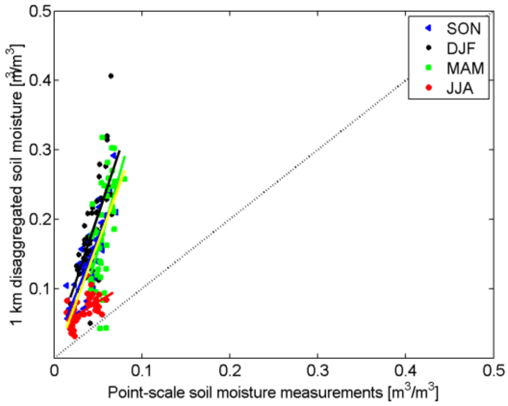

SON
DJF
MAM
JJA
1 km disaggregated soil moisture [m3/m3]
Point-scale soil moisture measurements [m3/m3]

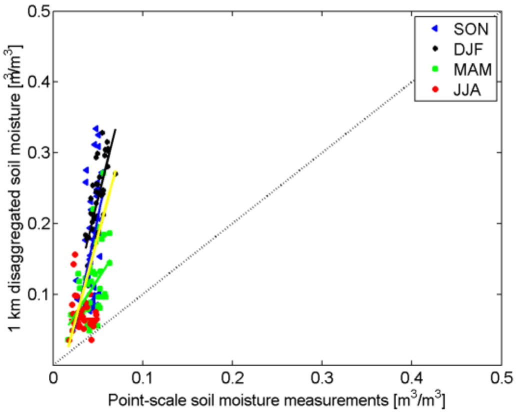

SON
DJF
MAM
JJA
1 km disaggregated soil moisture [m3/m3]
Point-scale soil moisture measurements [m3/m3]

J3 STATION

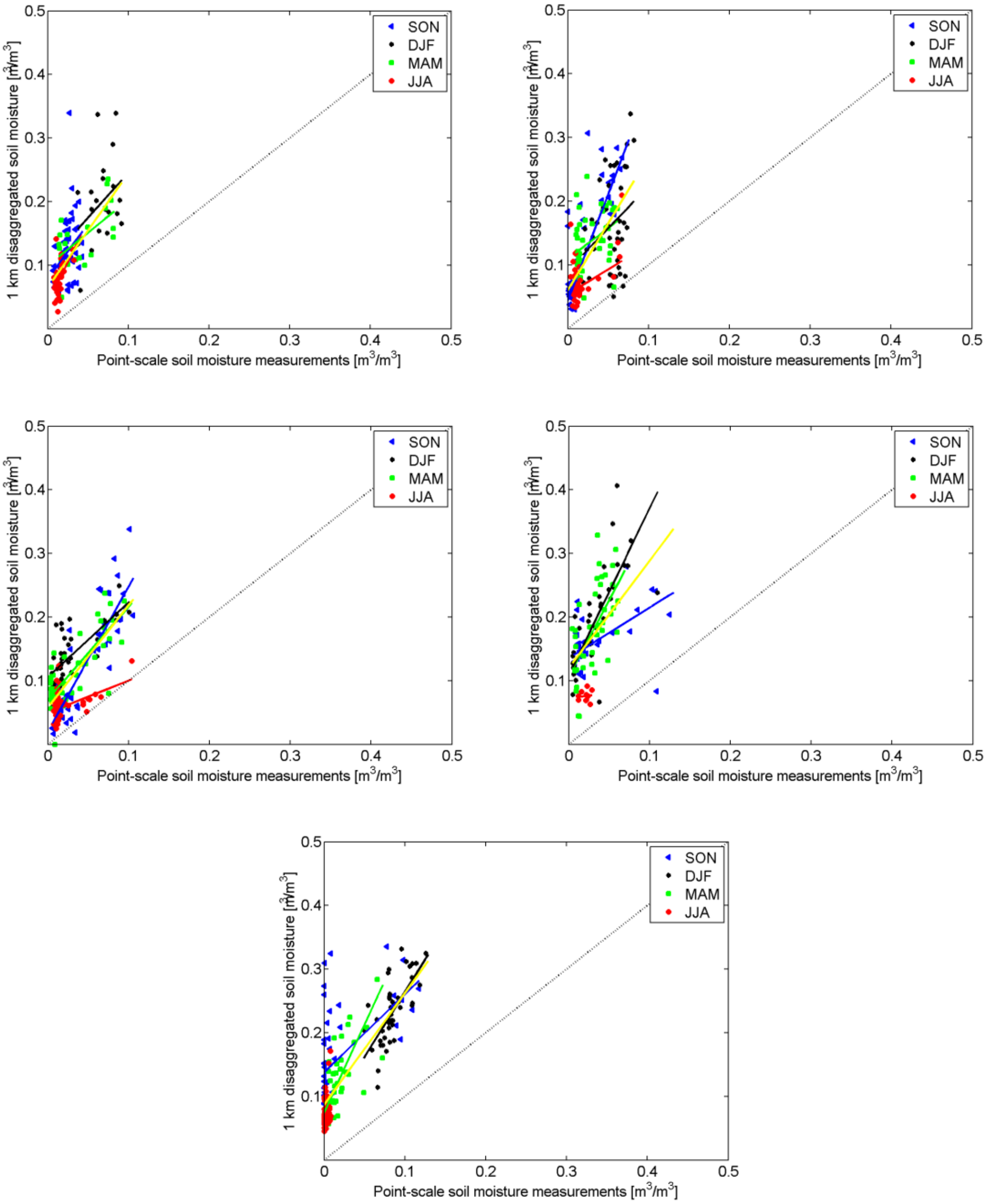
SON
DJF
MAM
JJA
1 km disaggregated soil moisture [m³/m³]
Point-scale soil moisture measurements [m³/m³]
0
0.1
0.2
0.3
0.4
0.5

J12 STATION

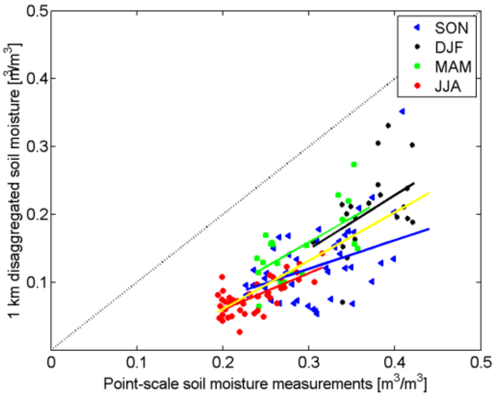
1 km disaggregated soil moisture [m³/m³]
Point-scale soil moisture measurements [m³/m³]
SON
DJF
MAM
JJA

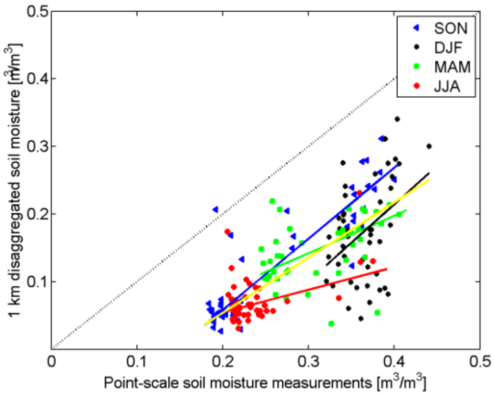
1 km disaggregated soil moisture [m³/m³]
Point-scale soil moisture measurements [m³/m³]
SON
DJF
MAM
JJA

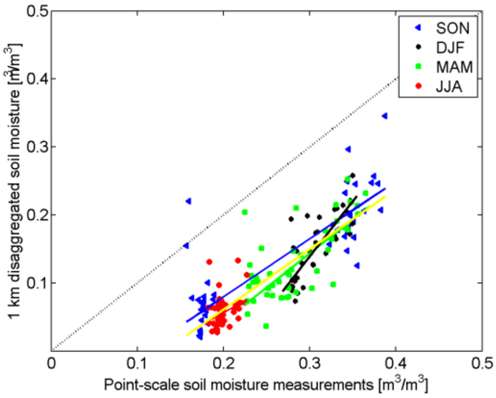
1 km disaggregated soil moisture [m³/m³]
Point-scale soil moisture measurements [m³/m³]
SON
DJF
MAM
JJA

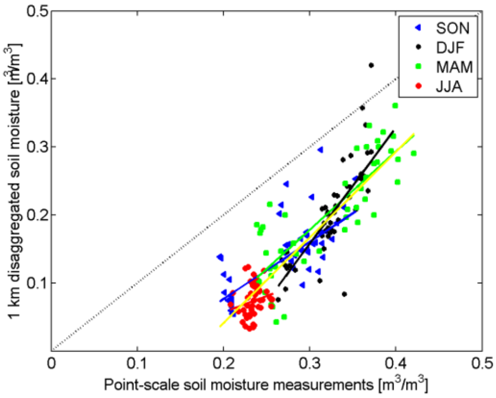
1 km disaggregated soil moisture [m³/m³]
Point-scale soil moisture measurements [m³/m³]
SON
DJF
MAM
JJA

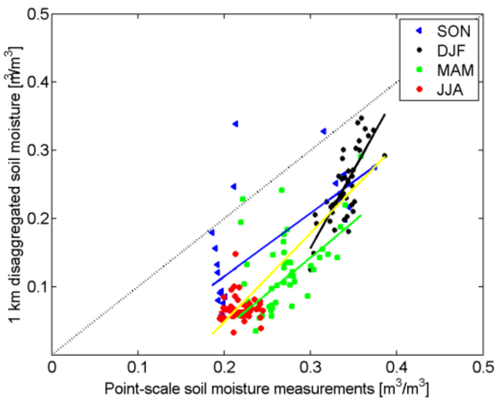
1 km disaggregated soil moisture [m³/m³]
Point-scale soil moisture measurements [m³/m³]
SON
DJF
MAM
JJA

K4 STATION

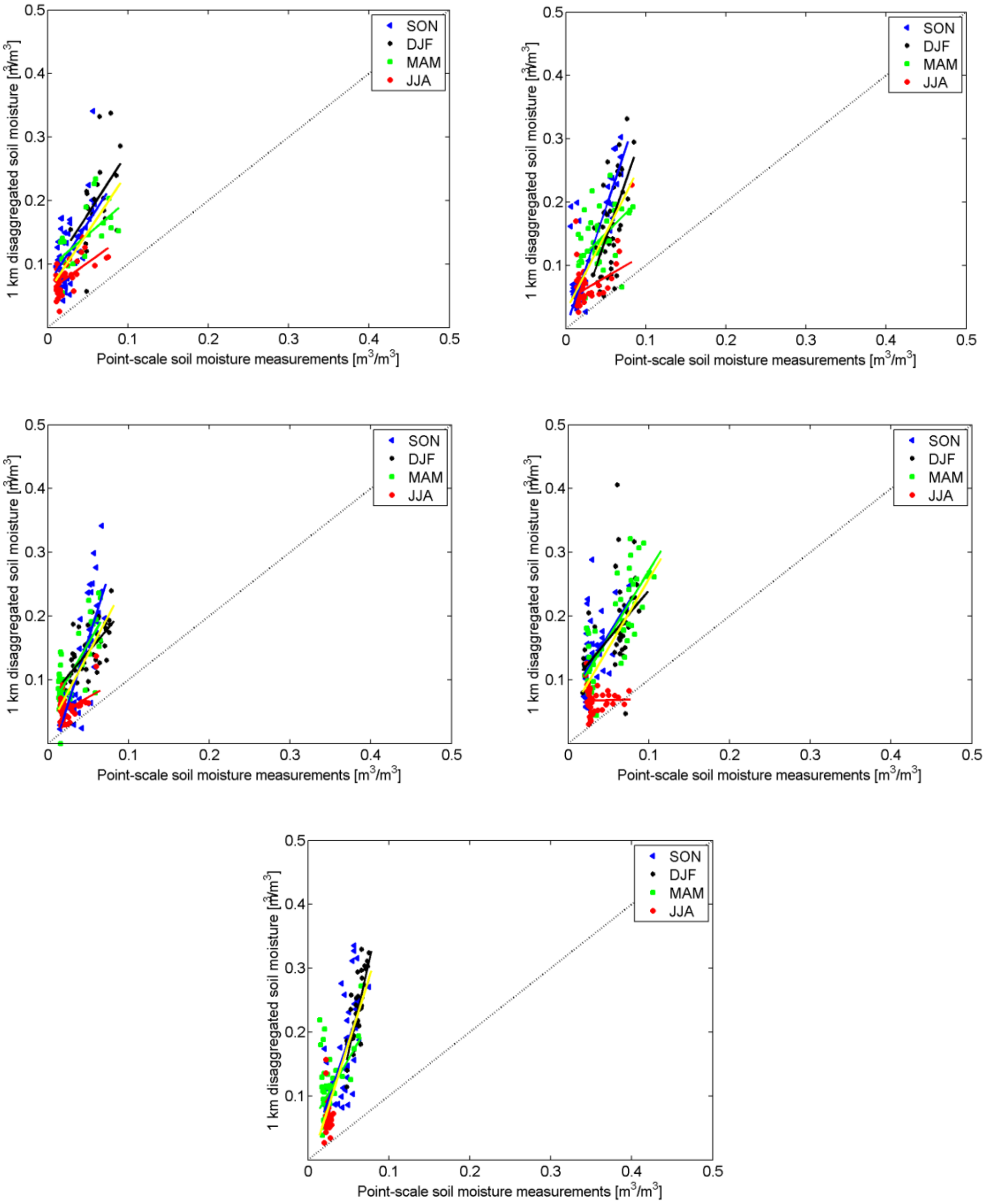
SON
DJF
MAM
JJA
1 km disaggregated soil moisture [m³/m³]
Point-scale soil moisture measurements [m³/m³]
0
0.1
0.2
0.3
0.4
0.5

K9 STATION

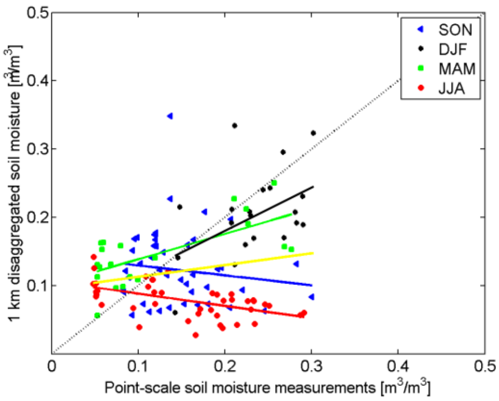
SON
DJF
MAM
JJA
1 km disaggregated soil moisture [m3/m3]
Point-scale soil moisture measurements [m3/m3]

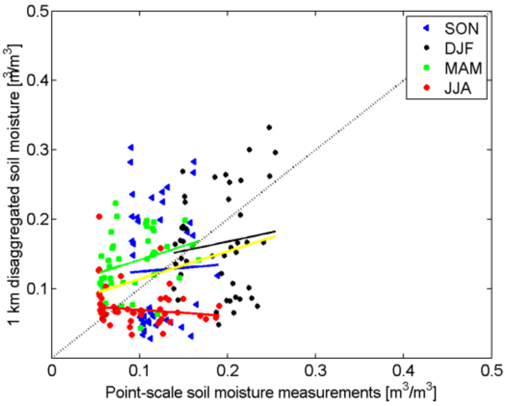
SON
DJF
MAM
JJA
1 km disaggregated soil moisture [m3/m3]
Point-scale soil moisture measurements [m3/m3]

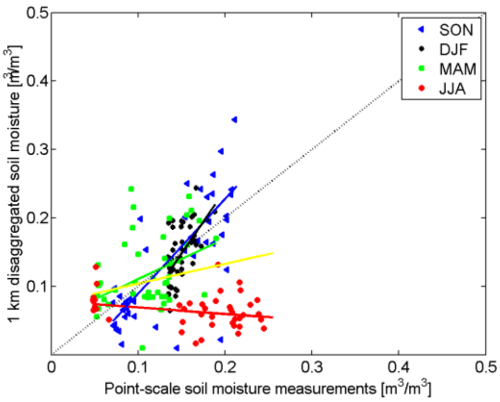
SON
DJF
MAM
JJA
1 km disaggregated soil moisture [m3/m3]
Point-scale soil moisture measurements [m3/m3]

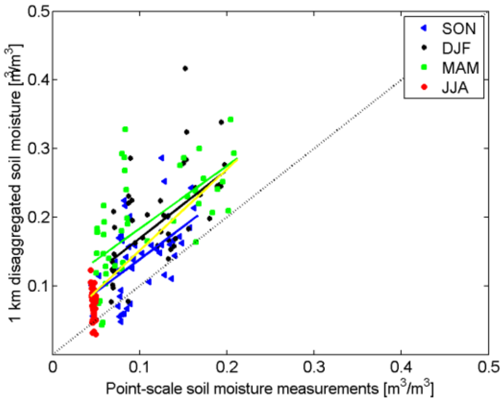
SON
DJF
MAM
JJA
1 km disaggregated soil moisture [m3/m3]
Point-scale soil moisture measurements [m3/m3]

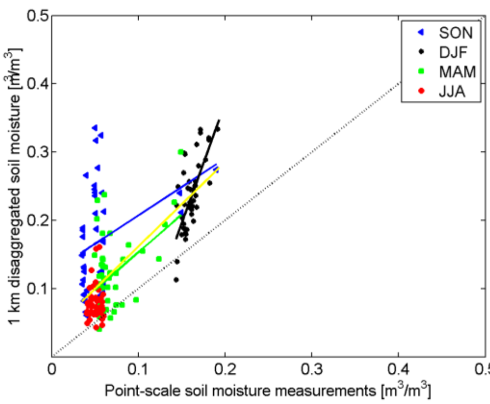
SON
DJF
MAM
JJA
1 km disaggregated soil moisture [m3/m3]
Point-scale soil moisture measurements [m3/m3]

K10 STATION

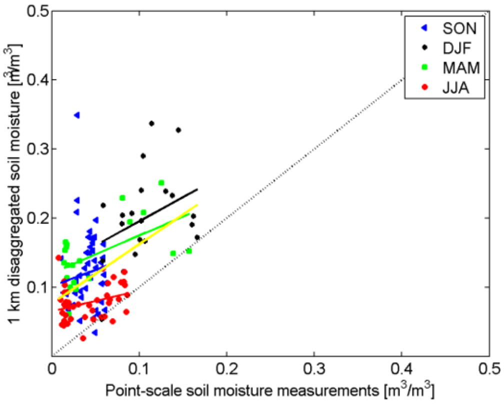
SON
DJF
MAM
JJA
1 km disaggregated soil moisture [m3/m3]
Point-scale soil moisture measurements [m3/m3]

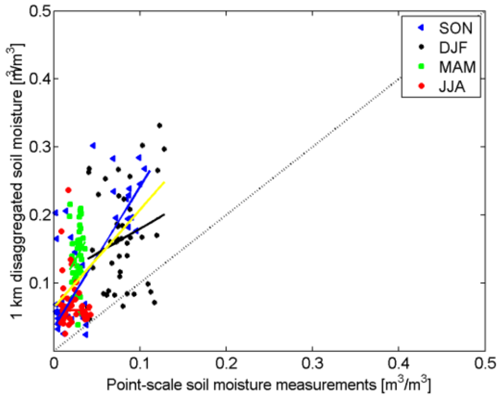
SON
DJF
MAM
JJA
1 km disaggregated soil moisture [m3/m3]
Point-scale soil moisture measurements [m3/m3]

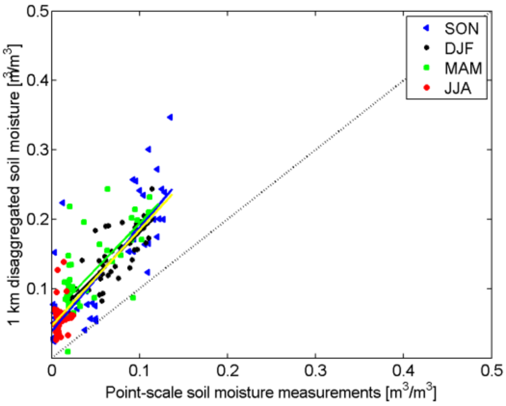
SON
DJF
MAM
JJA
1 km disaggregated soil moisture [m3/m3]
Point-scale soil moisture measurements [m3/m3]

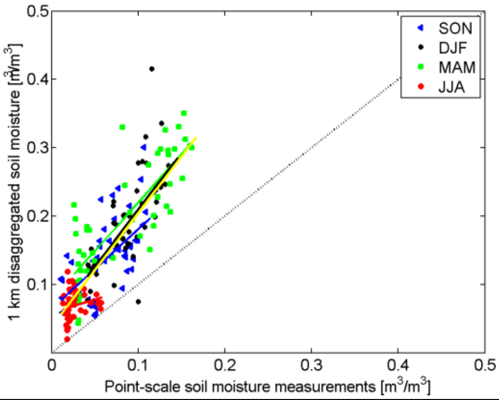
SON
DJF
MAM
JJA
1 km disaggregated soil moisture [m3/m3]
Point-scale soil moisture measurements [m3/m3]

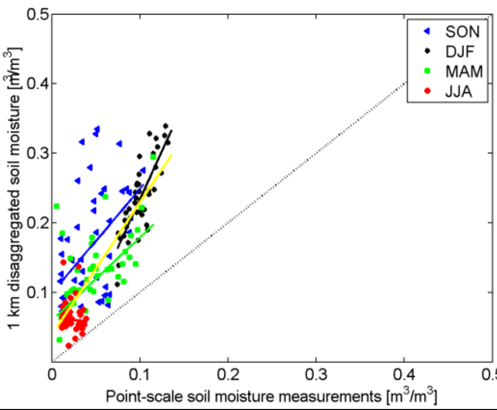
SON
DJF
MAM
JJA
1 km disaggregated soil moisture [m3/m3]
Point-scale soil moisture measurements [m3/m3]

K13 STATION

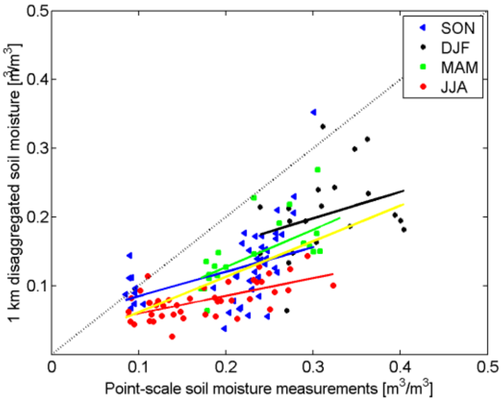

SON
DJF
MAM
JJA
1 km disaggregated soil moisture [m3/m3]
Point-scale soil moisture measurements [m3/m3]

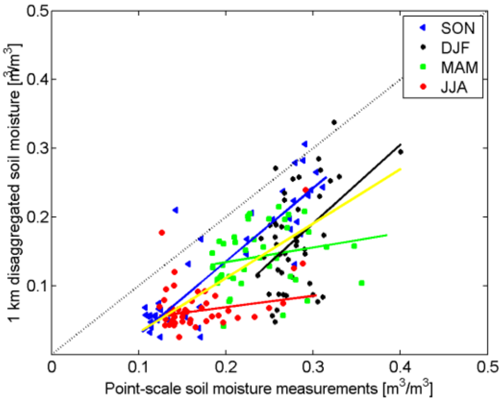

SON
DJF
MAM
JJA
1 km disaggregated soil moisture [m3/m3]
Point-scale soil moisture measurements [m3/m3]

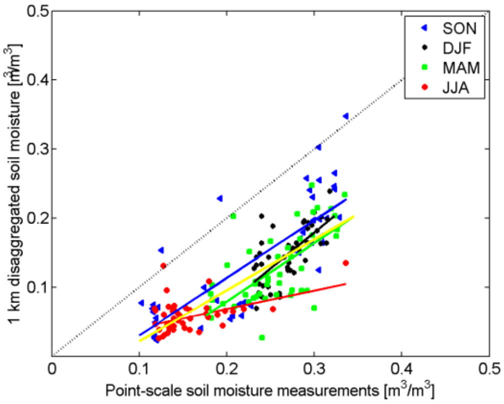

SON
DJF
MAM
JJA
1 km disaggregated soil moisture [m3/m3]
Point-scale soil moisture measurements [m3/m3]

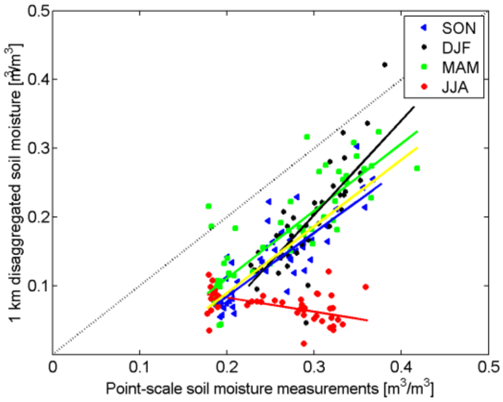

SON
DJF
MAM
JJA
1 km disaggregated soil moisture [m3/m3]
Point-scale soil moisture measurements [m3/m3]

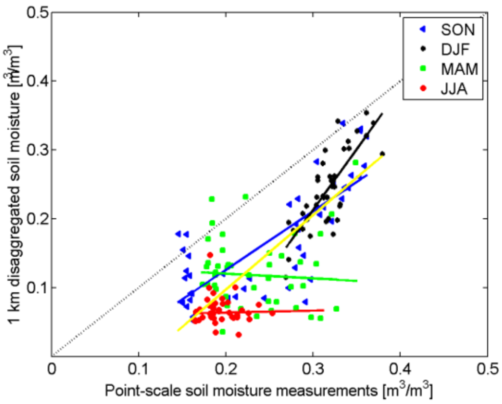

SON
DJF
MAM
JJA
1 km disaggregated soil moisture [m3/m3]
Point-scale soil moisture measurements [m3/m3]

L3 STATION

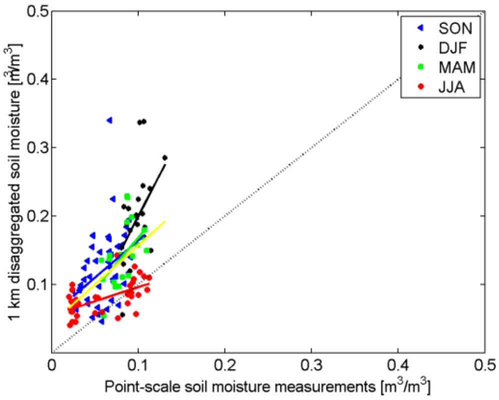
SON
DJF
MAM
JJA
1 km disaggregated soil moisture [m3/m3]
Point-scale soil moisture measurements [m3/m3]

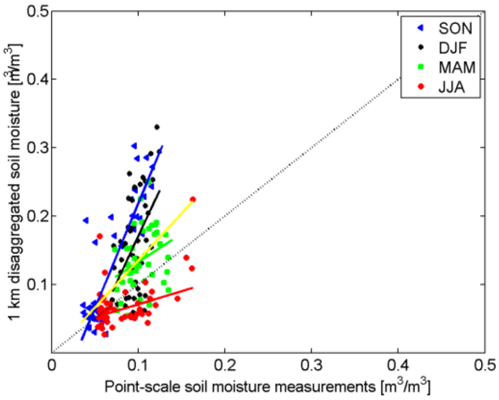
SON
DJF
MAM
JJA
1 km disaggregated soil moisture [m3/m3]
Point-scale soil moisture measurements [m3/m3]

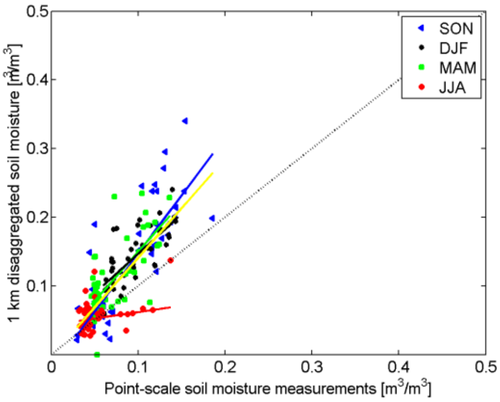
SON
DJF
MAM
JJA
1 km disaggregated soil moisture [m3/m3]
Point-scale soil moisture measurements [m3/m3]

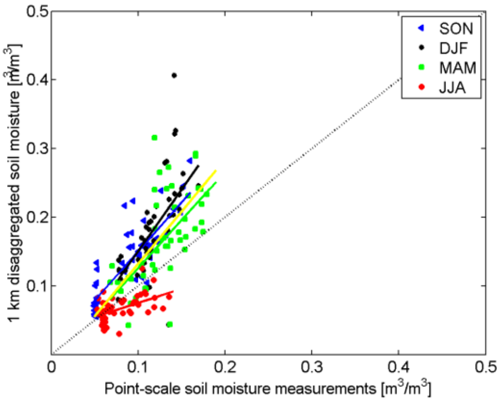
SON
DJF
MAM
JJA
1 km disaggregated soil moisture [m3/m3]
Point-scale soil moisture measurements [m3/m3]

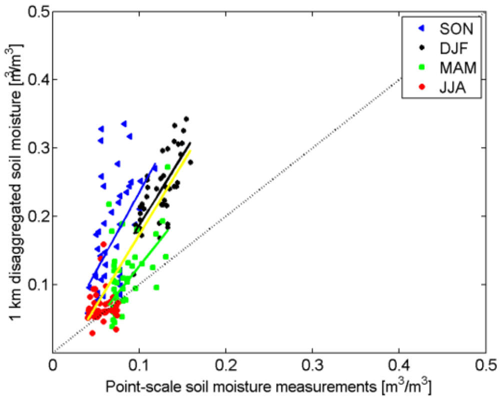
SON
DJF
MAM
JJA
1 km disaggregated soil moisture [m3/m3]
Point-scale soil moisture measurements [m3/m3]

L7 STATION

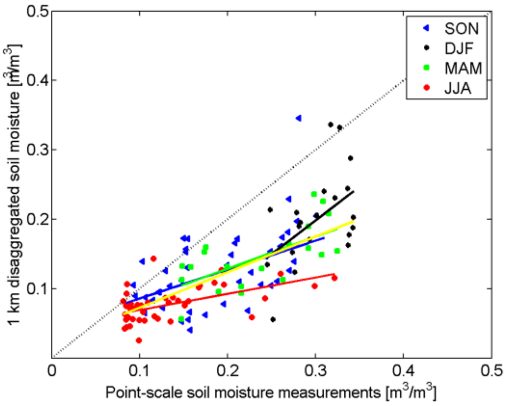

SON
DJF
MAM
JJA
1 km disaggregated soil moisture [m^3/m^3]
Point-scale soil moisture measurements [m^3/m^3]

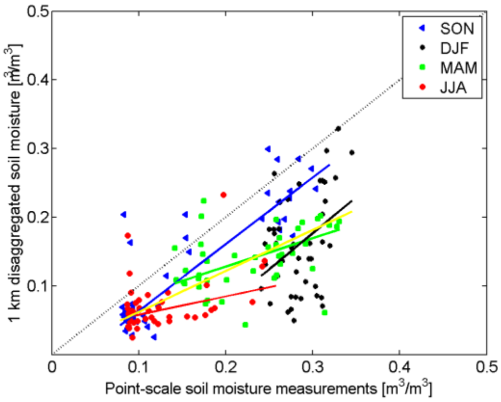

SON
DJF
MAM
JJA
1 km disaggregated soil moisture [m^3/m^3]
Point-scale soil moisture measurements [m^3/m^3]

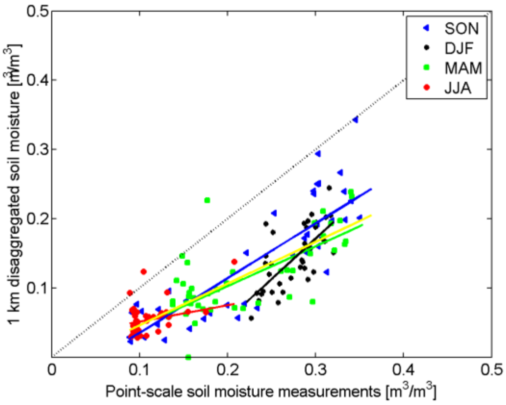

SON
DJF
MAM
JJA
1 km disaggregated soil moisture [m^3/m^3]
Point-scale soil moisture measurements [m^3/m^3]

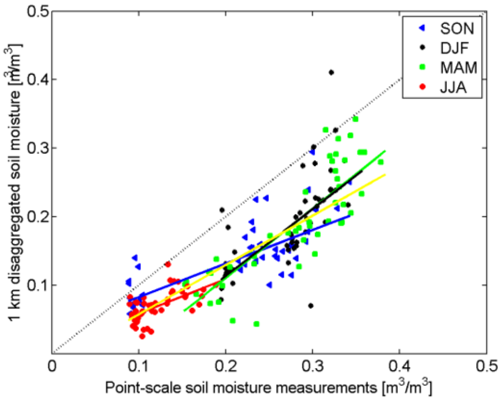

SON
DJF
MAM
JJA
1 km disaggregated soil moisture [m^3/m^3]
Point-scale soil moisture measurements [m^3/m^3]

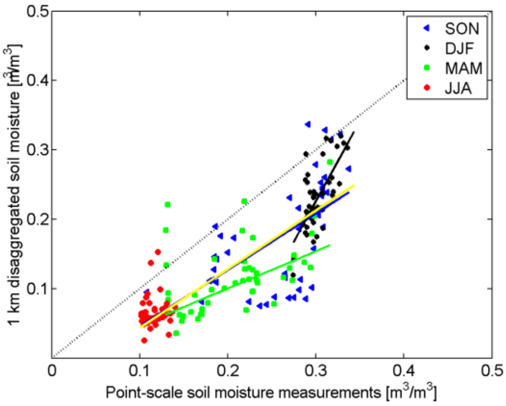

SON
DJF
MAM
JJA
1 km disaggregated soil moisture [m^3/m^3]
Point-scale soil moisture measurements [m^3/m^3]

M5 STATION

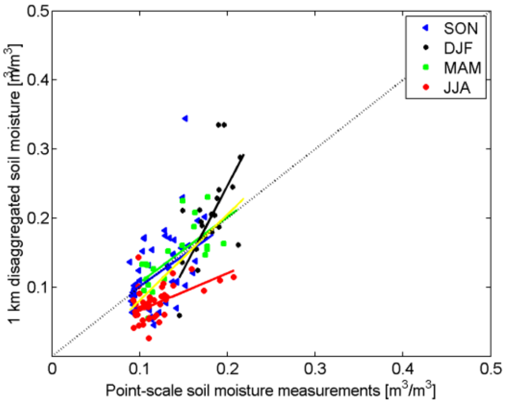

SON
DJF
MAM
JJA
1 km disaggregated soil moisture [m³/m³]
Point-scale soil moisture measurements [m³/m³]

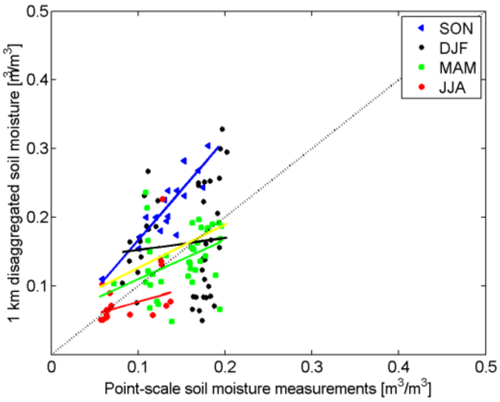

SON
DJF
MAM
JJA
1 km disaggregated soil moisture [m³/m³]
Point-scale soil moisture measurements [m³/m³]

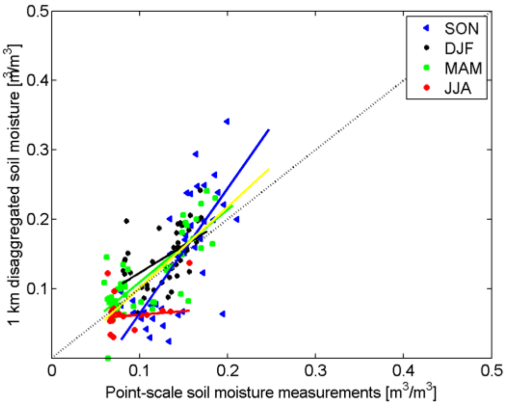

SON
DJF
MAM
JJA
1 km disaggregated soil moisture [m³/m³]
Point-scale soil moisture measurements [m³/m³]

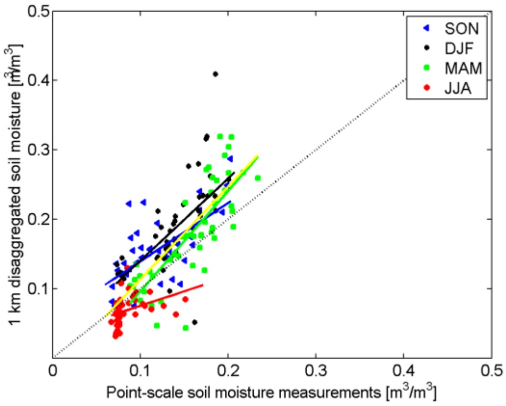

SON
DJF
MAM
JJA
1 km disaggregated soil moisture [m³/m³]
Point-scale soil moisture measurements [m³/m³]

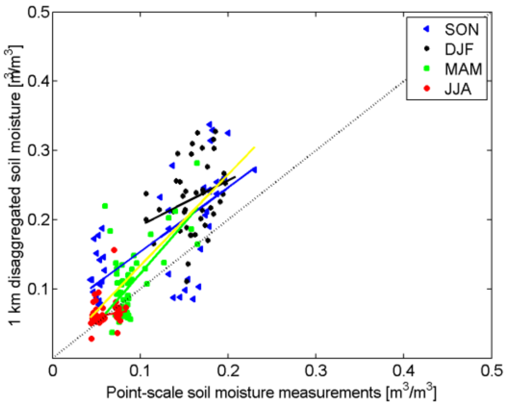

SON
DJF
MAM
JJA
1 km disaggregated soil moisture [m³/m³]
Point-scale soil moisture measurements [m³/m³]

M9 STATION

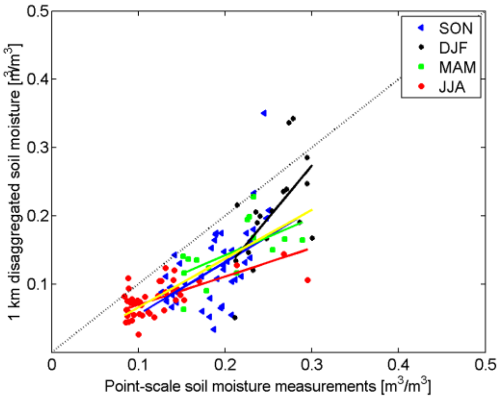
SON
DJF
MAM
JJA
1 km disaggregated soil moisture [m³/m³]
Point-scale soil moisture measurements [m³/m³]

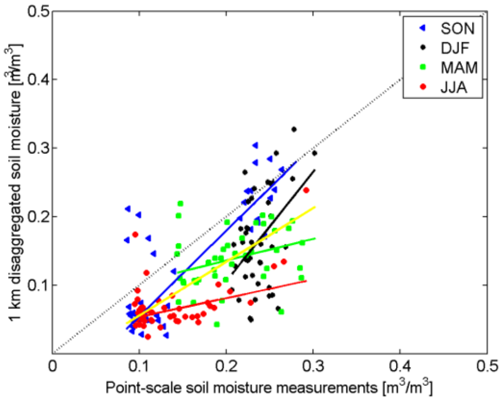
SON
DJF
MAM
JJA
1 km disaggregated soil moisture [m³/m³]
Point-scale soil moisture measurements [m³/m³]

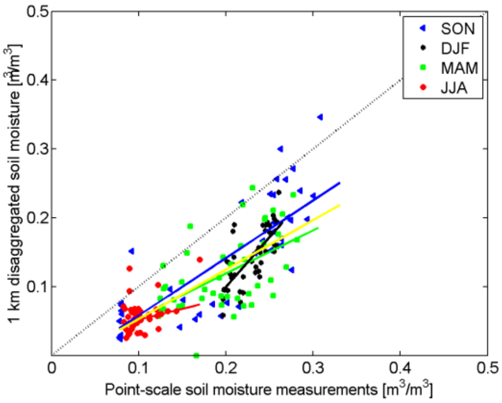
SON
DJF
MAM
JJA
1 km disaggregated soil moisture [m³/m³]
Point-scale soil moisture measurements [m³/m³]

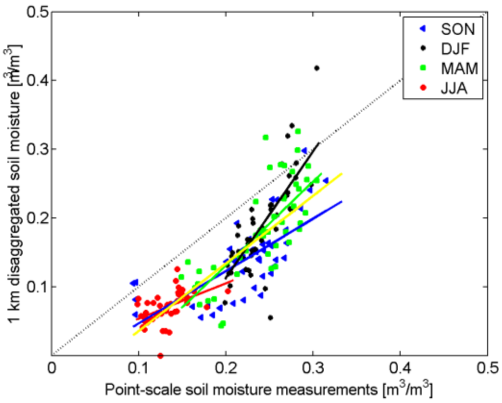
SON
DJF
MAM
JJA
1 km disaggregated soil moisture [m³/m³]
Point-scale soil moisture measurements [m³/m³]

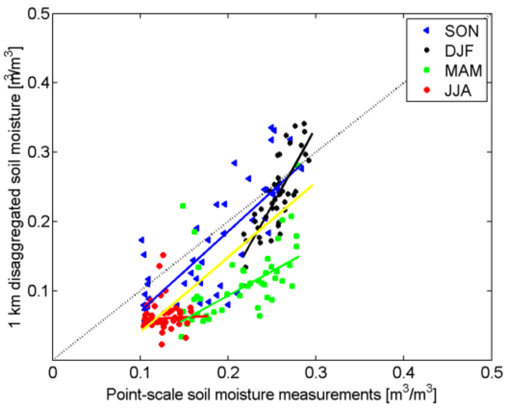
SON
DJF
MAM
JJA
1 km disaggregated soil moisture [m³/m³]
Point-scale soil moisture measurements [m³/m³]

M13 STATION

Year 2013 and 2014 do not have data, so last image belongs to year 2012.

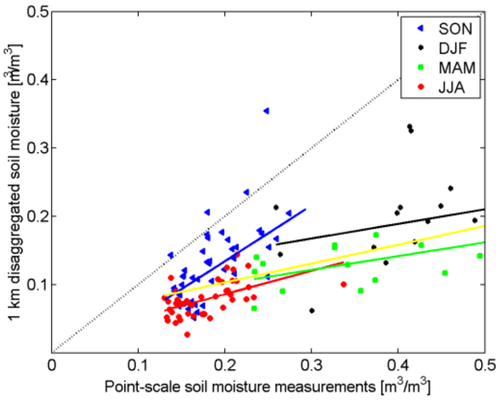

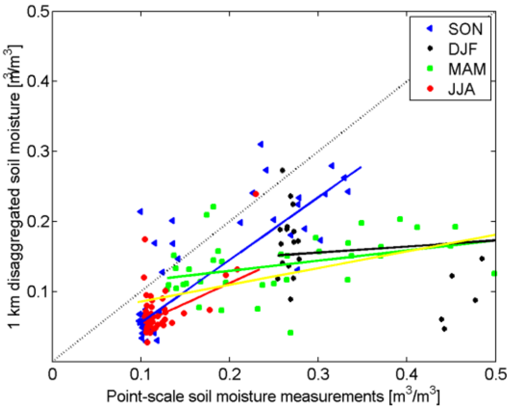

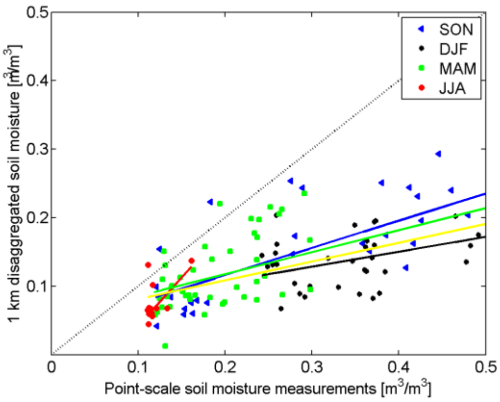

N9 STATION

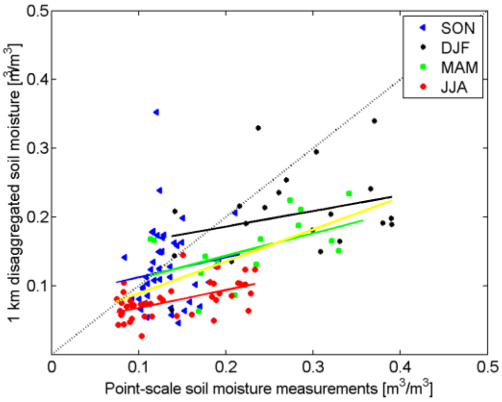

SON
DJF
MAM
JJA
1 km disaggregated soil moisture [m3/m3]
Point-scale soil moisture measurements [m3/m3]

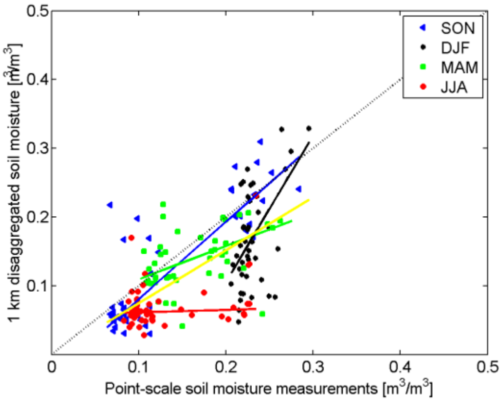

SON
DJF
MAM
JJA
1 km disaggregated soil moisture [m3/m3]
Point-scale soil moisture measurements [m3/m3]

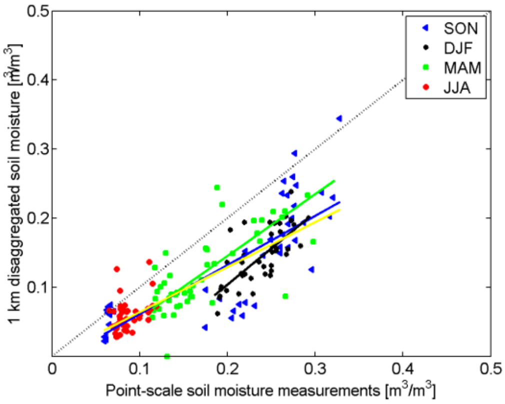

SON
DJF
MAM
JJA
1 km disaggregated soil moisture [m3/m3]
Point-scale soil moisture measurements [m3/m3]

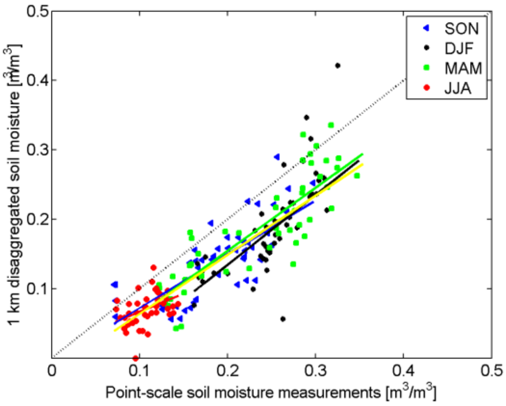

SON
DJF
MAM
JJA
1 km disaggregated soil moisture [m3/m3]
Point-scale soil moisture measurements [m3/m3]

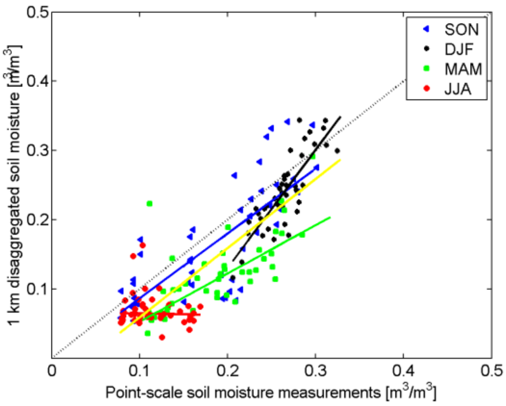

SON
DJF
MAM
JJA
1 km disaggregated soil moisture [m3/m3]
Point-scale soil moisture measurements [m3/m3]

O7 STATION

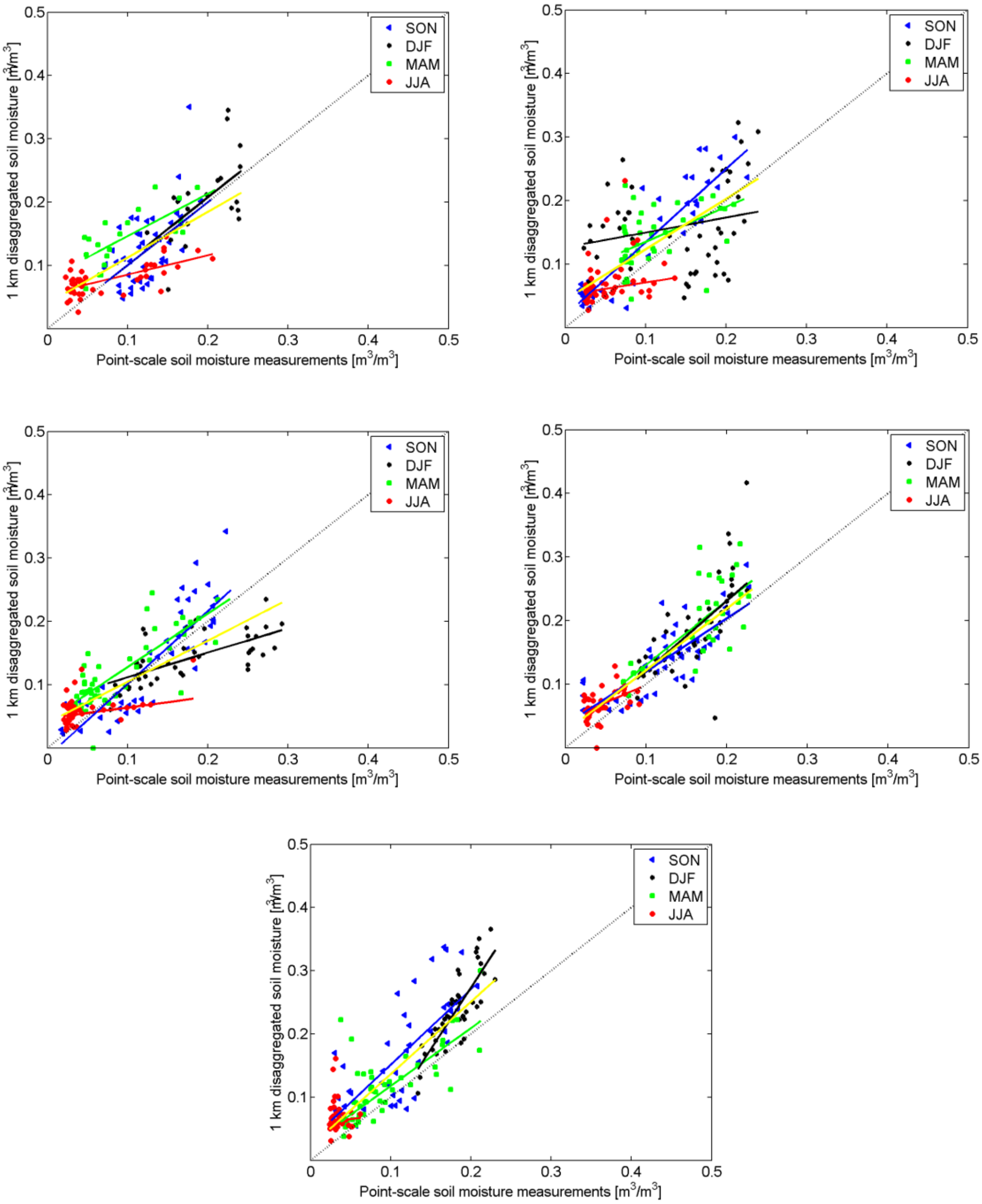

SON
DJF
MAM
JJA
1 km disaggregated soil moisture [m3/m3]
Point-scale soil moisture measurements [m3/m3]
0
0.1
0.2
0.3
0.4
0.5

COEFFICIENT MEDIANS

	a_1 (HR)					
	Problematic		Not problematic		All	
	Absolute value	Without absolute	Absolute value	Without absolute	Absolute value	Without absolute
2010	0.1785	0.1785	0.1921	0.1921	0.1916	0.1916
2011	0.1939	0.1939	0.2210	0.2210	0.2189	0.2189
2012	0.1981	0.1981	0.1946	0.1946	0.1950	0.1950
2013	0.1859	0.1859	0.2310	0.2310	0.2283	0.2283
2014	0.2160	0.2160	0.2339	0.2339	0.2318	0.2318

	a_2 (LST)					
	Problematic		Not problematic		All	
	Absolute value	Without absolute	Absolute value	Without absolute	Absolute value	Without absolute
2010	0.0457	-0.0249	0.0381	-0.0089	0.0566	-0.0110
2011	0.0377	- 0.0090	0.0413	-0.0198	0.0498	-0.0192
2012	0.0538	-0.0360	0.0481	-0.0187	0.0420	-0.0193
2013	0.0746	-0.0532	0.0493	-0.0339	0.0532	-0.0361
2014	0.0428	-0.0254	0.0518	-0.0315	0.0497	-0.0309

	a_3 (NDVI)					
	Problematic		Not problematic		All	
	Absolute value	Without absolute	Absolute value	Without absolute	Absolute value	Without absolute
2010	0.0025	-0.0013	0.0381	0.0093	0.0344	0.0057
2011	0.0025	-0.0008	0.0413	0.0215	0.0383	0.0176
2012	0.0022	-0.0002	0.0481	0.0325	0.0451	0.0290
2013	0.0032	0.0009	0.0493	0.0362	0.0465	0.0333
2014	0.0025	0.0001	0.0518	0.0458	0.0493	0.0413

	a_4 (TBH)					
	Problematic		Not problematic		All	
	Absolute value	Without absolute	Absolute value	Without absolute	Absolute value	Without absolute
2010	0.1439	-0.1439	0.1383	-0.1313	0.1383	-0.1313
2011	0.1838	-0.1775	0.1665	-0.1625	0.1714	-0.1649
2012	0.2285	-0.2285	0.1699	-0.1617	0.1711	-0.1652
2013	0.1130	-0.0902	0.1885	-0.1834	0.1842	-0.1816
2014	0.1348	-0.1348	0.1909	-0.1857	0.1901	-0.1849

	a_5 (TBV)					
	Problematic		Not problematic		All	
	Absolute value	Without absolute	Absolute value	Without absolute	Absolute value	Without absolute
2010	0.0709	0.0480	0.0681	0.0163	0.0681	0.0216
2011	0.0768	0.0285	0.0886	0.0308	0.0879	0.0295
2012	0.0963	0.0405	0.0963	0.0417	0.0971	0.0417
2013	0.0757	0.0070	0.0124	0.0245	0.0735	0.0233
2014	0.1183	0.0472	0.0777	0.0303	0.0799	0.0311